EOQ N°65
March 2000

meteorology – earthnet – remote sensing – solid earth – future programmes

ATSR Special Issue

Earth Observation Quarterly

The Along Track Scanning Radiometer (ATSR) Instruments on ERS-1 and -2

C.T. Mutlow, D.L, Smith & M.J. Murray

Space Science and Technology Dept., Rutherford Appleton Laboratory
Chilton, Didcot, Oxfordshire, OX11 0QX UK
Phone: +44-1235-446526, E-mail: c.t.mutlow@rl.ac.uk

This issue of EOQ is dedicated to the Along Track Scanning Radiometer instruments that are being flown as part of the payload of the ERS-1 and -2 missions.The primary mission of these sensors is to obtain sea surface temperature data sets for climate studies, but the high-quality image data collected by the instruments has application to a wide range of EO activities. Careful pre-flight and in-flight calibration is a major feature of the ATSR instruments and their data are particularly suited to applications where high radiometric accuracy and stability is required. Each of the ATSR instruments carries two infrared calibration targets, and the ATSR-2 and the future ATSR instruments carry an on-board visible calibration system for their visible channels. This article explains some of the features and advantages of the instruments and the data sets they produce.

In this Issue

European Space Agency
Agence spatiale européenne

Introduction

Since the early 1990s, ESA has flown Along Track Scanning Radiometer (ATSR) instruments on its satellites.

The ERS-1 mission carried the first infra-red-only ATSR (now referred to as ATSR- 1), ERS-2 carried the ATSR-2, an improved instrument also equipped with visible channels in addition to the infrared, and Envisat is due carry a further Advanced ATSR (AATSR) early in the new millennium.

The original ATSR-1 instrument was developed by a UK-led consortium of research institutes and universities from the UK, Australia and France to meet the needs of the climate community.

The ATSR instruments are second generation space radiometers. They exploit the multi-channel method pioneered in the Advanced Very High Resolution Radiometers (AVHRRs) flown on previous NOAA operational satellites, but also use new technology to improve instrument stability and calibration, detector noise performance, and to provide observations of the same surface scene at two different angles.

The ATSR sensors have been designed specifically to provide new information urgently needed for the debate on climate change and global warming, as well as to produce well-calibrated image data sets for use in a wide range of EO studies.

The ATSR Instruments

There are currently three ATSR instruments, as mentioned above, which all have a common specification, although there are some differences in implementation.

ATSR-1, launched as part of the payload of ESA's ERS-1 satellite on 17th July 1991, was the test-bed for the "along track scanning" concept. It carries infrared channels at 1.6, 3.7, 10.8 and 12.0 µm, and has no visible channels. The instrument operated from August 1991, until routine ERS-1 operations stopped (when the satellite was put into hibernation) in June 1996. Data from the 3.7 µm was not available after May 1992 when this channel failed.

The ATSR-2, for ERS-2, and Advanced ATSR (AATSR) instruments are developments of the ATSR-1 which, in addition to the standard ATSR infrared channels, carry visible channels for vegetation, aerosol and cloud remote sensing. These channels each have a spectral width of 20nm, and are centred at 0.55 0.67, and 0.87 µm, respectively. These narrow bands have been chosen to maximise the sensor's sensitivity, whilst avoiding significant atmospheric absorption features that would otherwise distort the signals from the ground. ATSR-2 is the current operational ATSR and is flying on the ESA ERS- 2 satellite which was launched in April 1995.

Further details of the ATSR-1 and 2 instruments are given in *Edwards et al*. [1990], *Gray et al*. [1991] and the 'ATSR User Guide' available from the project website <http://www.atsr.rl.ac.uk>.

The next instrument, AATSR, will be launched early in the millennium on ESA's Envisat platform, and has been funded by the UK Department of the Environment, Transport and the Regions, Natural Environment Research Council, and the Australian Department of Industry, Science and Resources in recognition of the need to provide continuity of the ATSR sea surface temperature (SST) data record for climate studies.

There was a significant overlap of the ATSR-1 and ATSR-2 missions, to allow cross-validation of the two sensors; it is expected that the ATSR-2 and AATSR missions will overlap similarly.

Features of the ATSR Instruments

The novel feature of each ATSR is the use of 'along track scanning' to provide observations of the same surface scene at two different angles through the intervening atmosphere (see Fig. 1).

By viewing the same scene through different atmospheric paths in this way, an accurate correction for the effects of the atmosphere on the surface measurement can be achieved. This correction is a substantial improvement over that obtained from a single-view measurement.

ATSR's field of view comprises two 512 km-wide curved swaths, with a nominal pixel size of 1 km^2 at the centre of the nadir swath, and 1.5 km – 2 km at the centre of the forward swath.This viewing geometry produces 512-km-wide high-resolution infrared and, from ATSR-2, visible images of the Earth's surface from which SST and other geophysical products can be retrieved.

Noise Performance and Calibration

The other key features of the ATSR instruments are their low-noise detectors, high-quality calibration and long-term stability.

The noise performance of both the flight ATSR instruments is extremely good, and even after several years in-flight ATSR-1 was achieving a better noise performance than is seen in typical AVHRR instruments soon after launch.

Early in the ERS1 mission, the ATSR-1 instrument's detector temperatures were at their coldest (at around 91 K) and their noise equivalent delta temperatures (NE∆T) were better than 50 mK. This deteriorated to an NE∆T of 60 mK in the 11 mm channel, and 130 mK in the 12 mm channel at the end of the sensor's operational mission. This increase in sensor noise is due degradation in the cooler performance which resulted in the temperatures of the IR detectors rising to over 110 K.

The in-flight NE∆T performance of the ATSR-2 detectors is much better than those in ATSR-1. The 11 mm channel achieves a typical NE∆T of 36 mK, and the 12 mm channel a typical NE∆T of 46 mK for a scene at 280 K. The noise performance of the ATSR-2 channels have not deteriorated with time, unlike those in ATSR-1, because the ATSR-2 cooler has been able to maintain the instrument's IR detectors at 81±1 K

The viewing geometry of the ATSR instrument.

1

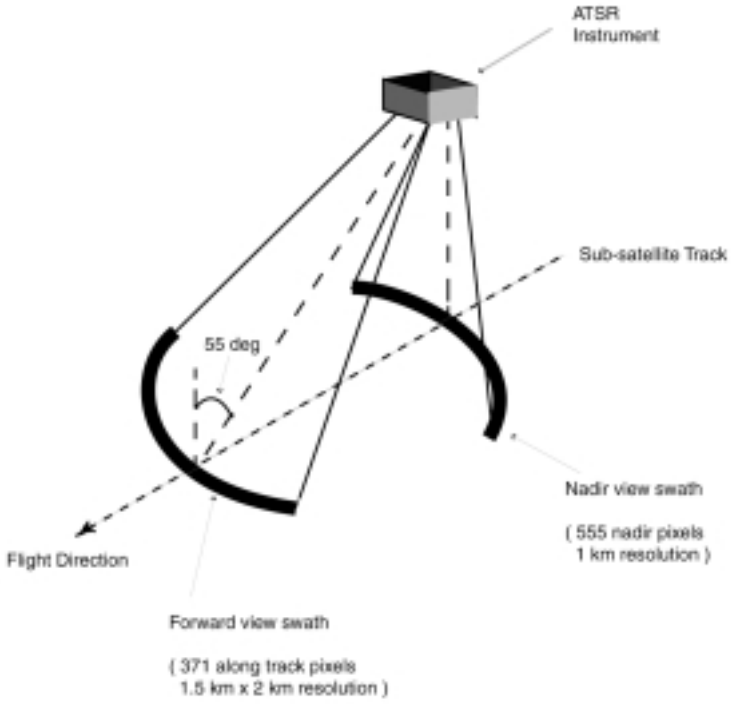

over the mission with an around orbit stability of ±0.1 K.

The ATSR-2 visible channels also have excellent radiometric performance, achieving 20:1 signal to noise ratios for signals corresponding to 0.5% albedo.

Each ATSR has been carefully designed, extensively calibrated and characterised on the ground before launch and, to maintain the high standard of its calibration after launch, includes stable state- of-the-art on-board calibration systems, which remove the need to rely on in-situ data for the calibration of the sensors.

ATSR's infrared channels are calibrated during each scan against a pair of black-body calibration targets spanning the expected range of SST; one target is cold, typically at -10°C, and the other hot at around +30°C. The infrared calibration is applied automatically during the ground processing so that users are provided with fully calibrated brightness temperatures (or SST) with all sensor non-linearities removed.

Calibration of the ATSR-2 (and AATSR) visible channels is achieved once during each orbit by viewing the Sun using a Russian Opal diffuser. However, due to ground processing constraints, the visible channel calibration is not performed as part of the automatic processing. Instead the visible calibration coefficients are provided for users at <http://www.atsr.rl.ac.uk/calibration.html> on the ATSR project website.

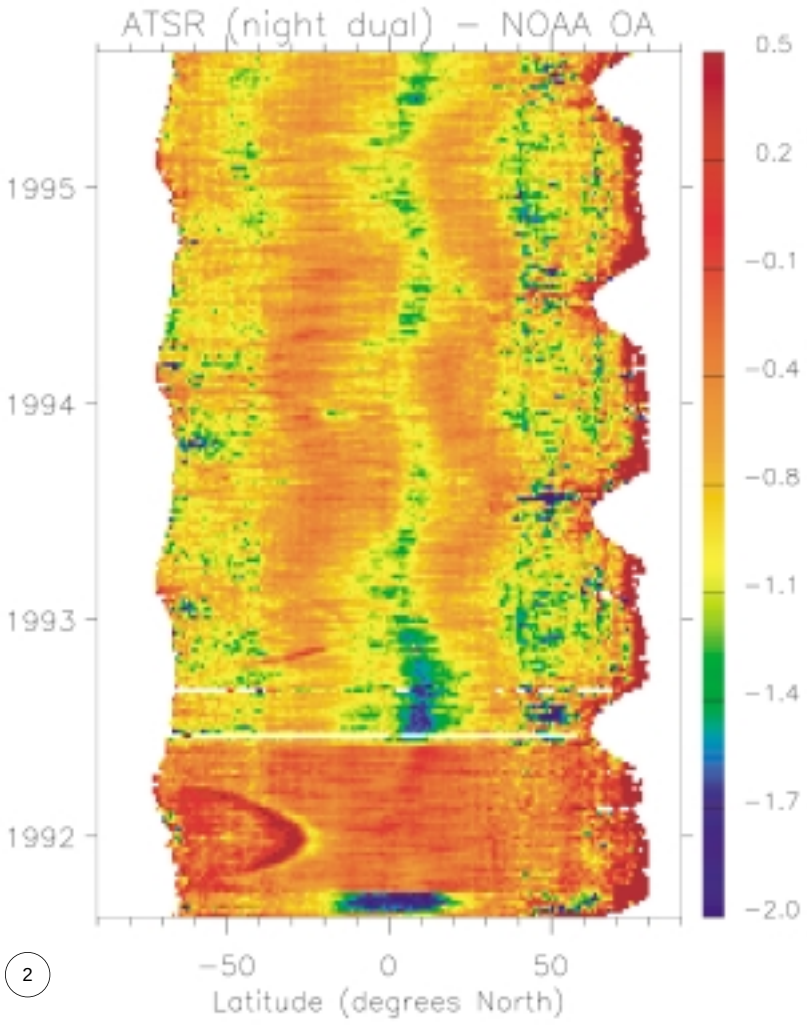

2

Zonal mean of the difference between the ATSR dual view night time SSTs and NOAA blended analysis.

Comparisons With AVHRR SST Data

Infrared radiometers like ATSR observe the emission from, and hence the temperature of, the water layer within 0.1 mm of the surface. The temperature of this layer is typically several tenths of a degree colder than that of the 'bulk' ocean a few millimetres beneath, and is known as the 'skin' temperature.

The ATSR SST data are provided as a 'skin' temperature rather than the pseudo-bulk temperatures that are provided by the AVHRR method of regressing satellite observations to buoy SST [*see Mutlow et al*., 1994, *Zavody et al*., 1995, and *Murray et al*., 1998 for further discussion of this]. This approach has the advantage that, although the SST retrieval scheme includes climatological atmospheric data, the ATSR SST data set, unlike AVHRR, is independent of the in-situ bulk observation data set.

Considerable work has been done to val-idate the SST retrievals from the ATSR instruments through comparison with other data sets, including the NOAA blended analysis of AVHRR and in situ observations. Recent results from ATSR-1 [*Murray et al*., 1998] demonstrate that during the Mt. Pinatubo eruption the ATSR SST retrievals using the dual views at 3.7, 10.8 and 12.0 µm are relatively insensitive to the state of the atmosphere. Figure 2, taken from *Murray et al*., shows the zonal mean of the difference between the ATSR dual-view night time SSTs and NOAA blended analysis. Aerosol contamination caused by the Mount Pinatubo plume (equatorial region) is apparent both at the start of the mission and following the failure of the 3.7 µm channel in May 1992. However, almost complete elimination of the Pinatubo aerosol is achieved during the nine-month period when ATSR 3.7 µm data are available (September 1991-May 1992).

It is clear from all the work undertaken that the ATSR instruments are delivering high quality 'skin' SST data, and that

3

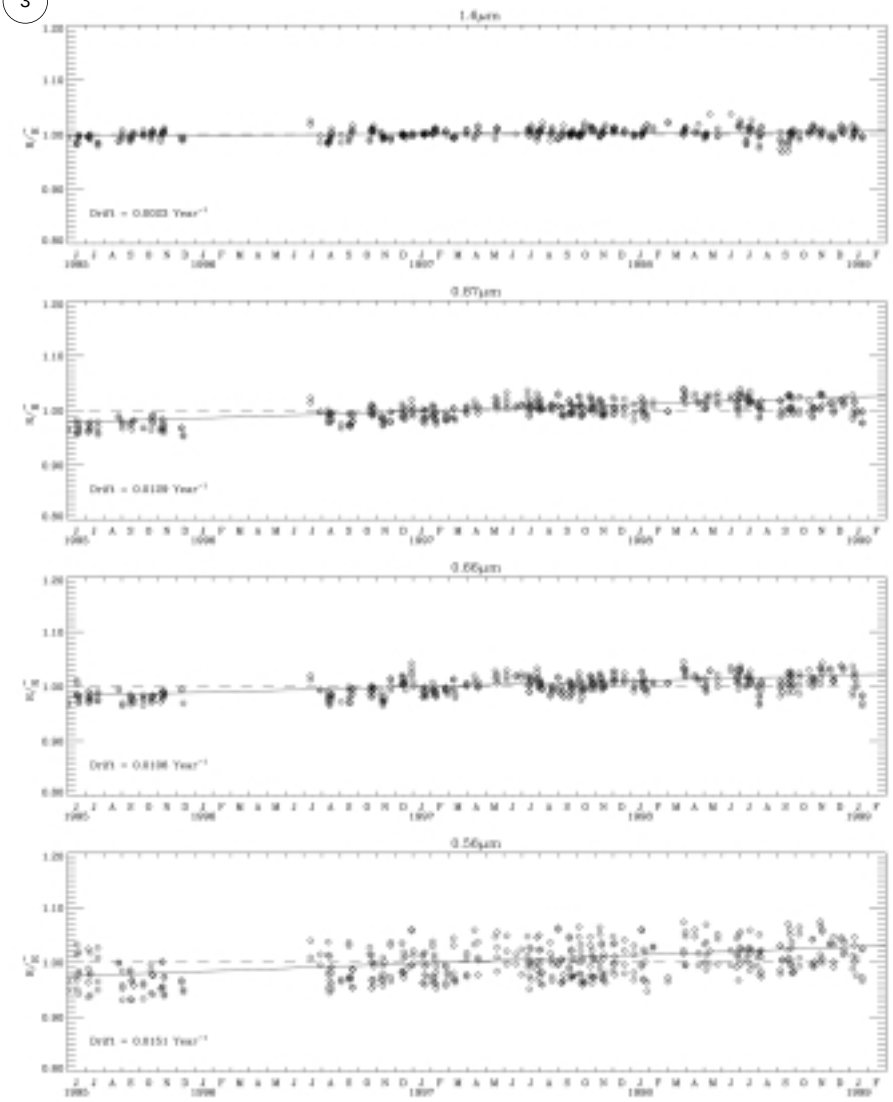

Normalised reflectances vs. time for an area of the eastern Saharan Desert showing the gradual drift in the ATSR-2 calibrated reflectances. the solid line is the result of fitting the drift function D = exp(k(t-t0)/365)) through these data.

the technique of along track scanning brings considerable benefits, particularly when 3.7 µm channel data are available, and is much less sensitive to errors in the modelling of atmospheric transmission than is the case for a nadir-only viewing instrument.

The ATSR-2 Visible Channels - Their Calibration and Stability

As well as the full complement of ATSR- 1 SST channels, ATSR-2 carries three additional visible channels at 0.55, 0.67 and 0.87 µm each with a spectral width of 20nm. To calibrate these channels ATSR-2 carries a prototype on-board vis-ible calibration system which has so far worked well, and which also has the potential to improve the calibration of other sensors.

Smith et al. [1997] describe a long series of observations from an area of the east-ern Saharan Desert on the Sudan/Egypt border, a site particularly favoured by NOAA for the calibration of the AVHRR visible channels [*Rao and Chen*, 1995]. The long-term stability of this site has to be assumed in the AVHRR calibration scheme, so quantifying the variability of the site is crucial to the reliability of the AVHRR calibration. *Smith et al*. [1997] have used calibrated ATSR-2 image data from the Libyan and several other ground sites to establish limits on the stability of the ATSR-2 on-board calibration system, and in turn on the seasonal variability of the Libyan desert site (see Fig. 3).

Similar studies are now in progress for a number of other test sites that cover a wide range of geographic locations and surface types, from Greenland snow to deserts in China. So far, these studies have confirmed the initial ATSR-2 calibration drifts derived from the Libyan desert work, and shown that at some sites the natural variations are so large that they are not suitable as vicarious calibration targets. Through this work, the calibration information obtained by ATSR-2 is being used to improve the understanding, and, hence, the quality of data from other sensors which have no on-board calibration and must rely on vicarious calibration methods.The accuracy of the retrieved surface reflectances are further improved by utilising the dual-view to obtain aerosol optical thick-nesses [*Mackay et al*., 1995].

The Future

The work presented in this paper describes the capability of the ATSR instruments to produce improved data sets through advances in calibration and the advantages of along track scanning for providing a robust atmospheric corrections. These data can be used to tackle new areas of science, and through synergistic use of ATSR data with information from other sensors will also bring benefits to other data sets by improving their calibration and reducing uncertainties in data interpretation.

The continuity of the ATSR-1 and -2, data set is assured by the AATSR which will be launched on ESA's Envisat satellite during 2001. AATSR carries the same channel complement as ATSR-2, and uses the same proven on-board calibra-tion methods for its visible and infrared channels.

References
Edwards, T., *et al.*, The along track scan-ning radiometer measurement of sea surface temperature from ERS-1, *J. Br. Interplanet. Soc.*, **43**, 160-180, 1990.

Gray, P.F. *et al.*, The optical system of the along track scanning radiometer MK ll (ATSR-2), *Proc. of ICSO '91*, Toulouse, 1991.

Mackay, G., Steven, M.D., & Clark, J.A., An tamospheric correction procedure fro the ATSR-2 visible and near-infrared land surface data, *Int. J. Remote Sens.*, **19**, 2949-2968, 1998.

Murray, M.J, Allen, M.R., Mutlow, C.T., Zavody, A.M., Jones, T.S. & Forrester, T.N., Actual and Potential information in dual-view radiometric observations of sea surface temperature from ATSR, *J. Geophys. Res.*, **103**, 8153-8165, 1998.

Mutlow, C.T., Zavody, A.M., Barton, I.J. & Llewellyn-Jones, D.T., Sea surface temperature measurements by the along track scanning radiometer on the ERS-1 satellite: Early results, *J. Geophys. Res.*, **99**, 575-588, 1994.

Rao, C.R.N, & Chen, J., Inter-satellite calibration linkages for the visible and near infrared channels of the Advanced Very High Resolution Radiometer on the NOAA-7, -9 and -11 spacecraft, *International Journal of Remote Sensing*, **16**, 1931-1942, 1995.

Smith D.L., Read P.D. & Mutlow C.T., The Calibration of the Visible/Near Infra-Red Channels of the Along-Track Scan-ning Radiometer-2 (ATSR-2) in Sensors, Systems and Next-Generation Satellites, Hiroyuki Fujisadsa, Editor, *Proceedings of SPIE*, **3221**, 53-62, 1997.

Zavody, A.M., Mutlow, C.T. & Llewellyn-Jones, D.T., A radiative transfer scheme for SST retrieval for the ATSR, *J. Geophys. Res.*, **100**, 937-952, 1995.

Zavody, A.M., Mutlow, C.T. & Llewellyn-Jones, D.T., ATSR Cloud clearing over ocean in the processing of data from the along-track scanning radiome-ter (ATSR), *Accepted for publication by the J. of Atmos. Ocean. Technol.*, 1999.

The New ESA/ESRIN ATSR Near-Realtime Service: Development, Operations and Data Distribution

A. Buongiorno, P. Goryl & E. Doyle

ESA/ESRIN Directorate of Application Programmes, Earth Observation Applications Department
V.Galileo Galilei 00044 Frascati, Italy
E-mail; abuongio@esrin.esa.it, pgoryl@esrin.esa.it, edoyle@esrin.esa.it

ESA/ESRIN has developed a Near Realtime (NRT) acquisition and processing system for the low-rate data which is acquired from the ATSR instrument onboard the ERS-2 satellite. To get the maximum world coverage from the same facility, the ATSR NRT system was installed at the Tromsø Satellite Station (TSS) in Norway, which was previously used for an ERS-1 ATSR-1 near realtime project.Different from a previous project, the current service is aimed to provide both full- and averaged-resolution products in near-realtime to remote users. All products are visible worldwide immediately after their generation and are made available for online downloadeding through a dedicated ATSR NRT WWW interface.

Introduction

The ATSR Near-Realtime system was conceived by ESA/ESRIN to provide the EO user community with access to ATSR data products within a short time after sensing. Thanks to the ERS satellite on-board recording capacity of low bit-rate data streams, it has been possible to acquire 10 of approximately 14 daily orbits (Fig. 1) from a single high-latitude station, located in Tromsø (N). The ATSR instrument, for its spectral and spatial characteristics, and for its revisiting frequency, is a suitable means for providing an operational monitoring of Earth's environment from the space. Severe environmental events which occurred recently, like extensive forest fires, smoke haze, flooding, etc., have clearly indicated that Earth-observing satellites play an important role in the various phases of disaster management [*Reports of International IDNDR Conference*, 1998]. In particular, the necessity for fast access to customised data and validated information has always been desired by the user community [*Buongiorno et al.*,1997]. Although current remote sensing space-borne systems are not always directly suitable for the monitoring of such events, we retain this experience as an opportunity to demonstrate to the user community closer the potential of using environmental satellites, and to provide important input for focussing the objectives and improving the capability of future Earth Observation missions.

ATSR NRT Data Processing

During the average 100-minute time interval between the acquisition of two

1

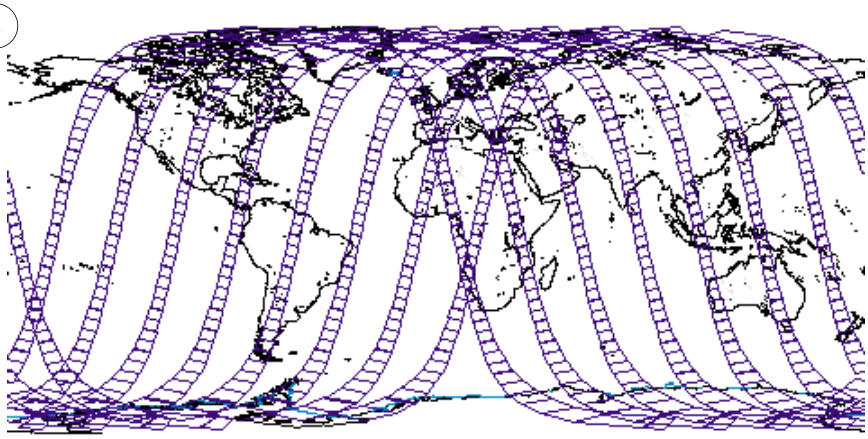

Example of an ATSR daily-coverage map for ascending and descending orbits downloaded to the Tromsø Satellite Station.

consecutive ERS-2 orbits, there are several steps of processing which have to be performed before providing the final products (Fig.2).

The first step consists of data ingestion and pre-processing, in which the ERS-2 low bit-rate data stream (15 Mbit/s) are acquired by a Direct Ingestion System (DIS) that performs the frame synchronisation of realtime and play-back data. After having reversed the play-back data, the ATSR instrument raw data are extracted, and sent to the NRT processing and control system which formats the ATSR source packets and groups them into half-orbital segments.

When a new half-orbit data set has been created, it is placed on a Digital Linear Tape (DLT) media for immediate ingestion into the ATSR data processor.

This processing is performed on a dedicated system running the SADIST application (a Synthesis of ATSR Data Into Sea-Surface Temperature) processor developed by Rutherford Appleton Laboratory (RAL). In parallel to SADIST processing, ATSR browse products are generated on the ATSR Browse generation System (ABS) [*Buongiorno*,1996].

When all the products are created, they are placed on an ATSR Dissemination

2

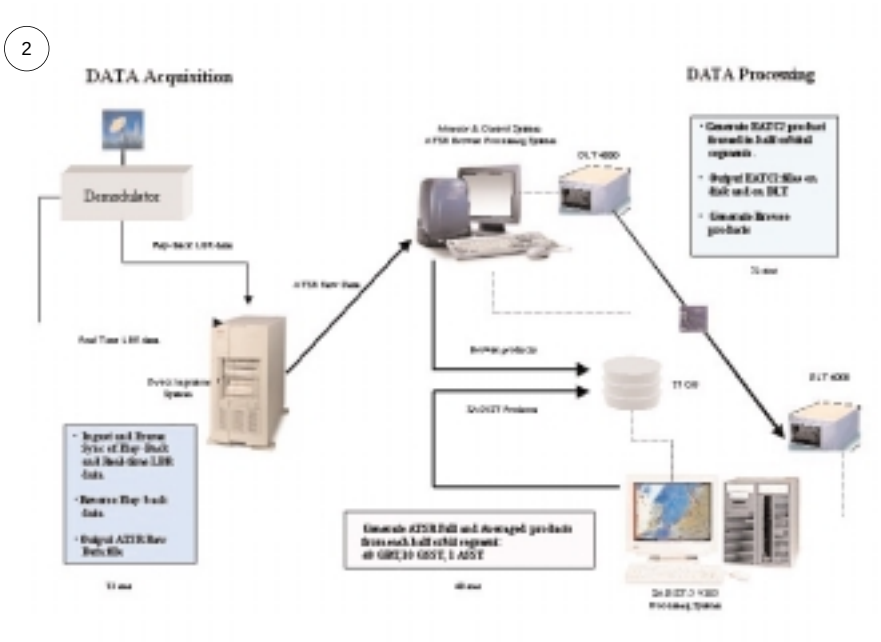

An overview of the ATSR NRT system for data processing.

System,which is visible to remote users (Fig.3). The ATSR full-resolution products are split into sub-parts and organised in a 6-day, rolling online archive, which corresponds to about 4800 ATSR products.

ATSR Products Available in NRT

The ATSR NRT system is designed to provide, in near-realtime, two classes of standard ATSR products [*Baily*, 1995], namely: averaged-resolution and gridded full-resolution.

Averaged-resolution products provide geophysical data organiszed in half- and tenth-degree latitude and longitude cells, and include three product types: ASST, ACLOUD and ABT. Contrary to averaged products distributed offline elsewhere, the NRT products always have a half-orbit length. This option has been chosen in order to ensure consistency with the processing and with the online archive organisation necessary for efficient browsing of the data.

Gridded products processed in NRT are of GBT (Gridded Brightness Temperature and reflectance) and GSST (Gridded Sea Surface Temperature) types. They consist of rectified ATSR scans in along track and across track coordinates framed in 512x512 lines/ pixel at 1-km resolution. A browse product is created from each half-orbit segment and then copied to the dissemination system where it is framed according to the spatial extension of GBT and GSST products, with the extraction of all auxiliary information.

The browse product is aimed at providing the end user with information and quick visibility of the ATSR full-resolution data, by presenting the main image features like cloud cover, land/sea cover, sunglint, data quality and geo-reference grid. All ATSR full-resolution products generated by the NRT system are optionally split into sub-parts before being put online in order to optimise data transfer and to allow users to customise the downloading of instrument data types according to their needs. The time required from instrument sensing to the availability of online

3

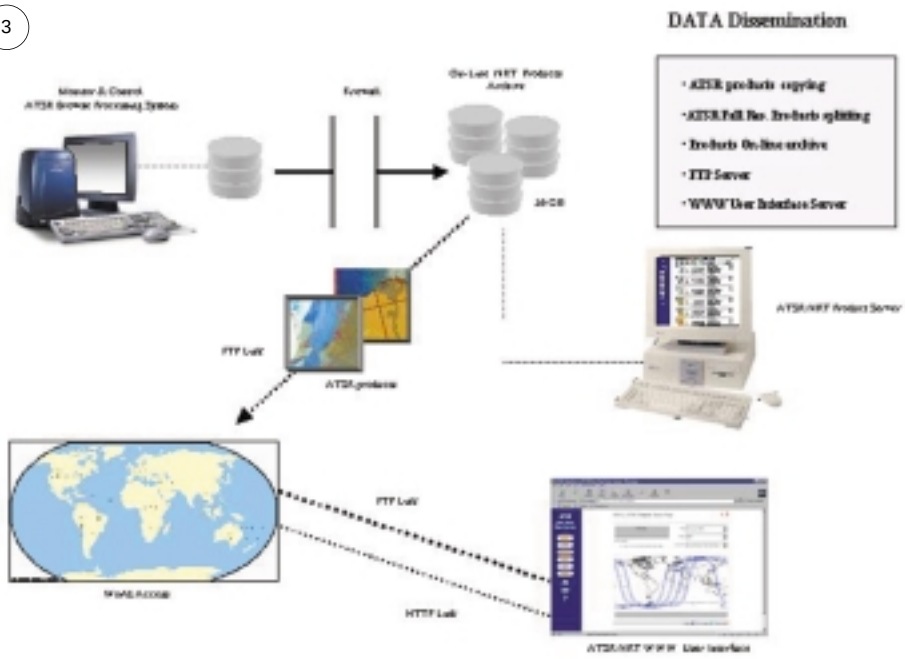

An overview of the ATSR NRT system for data dissemination.

products, ranges from about 1.5 to 3.5 hours. The time difference explained by the fact that each acquisition includes not only realtime sensing data, but also the on-board recorded data sensed in the previous 100 minutes.

ATSR NRT User Interface

To provide visibility and for the retrieval of ATSR NRT products, a dedicated WWW user interface has been developed (Fig.4) and is now available at: <http://192.111.33.173/ATSRNRT/>. The WWW interface provides data flow in real time by dynamically updating (every 10 minutes) all information and hyperlinks about new products. An interactive world map shows the footprint of the products and enables their selection. In this simple way, the user has the visual control of the acquired data and, at the same time, their geographic location.

The products selected from the map are presented as into 'result pages' from where more details are available. At this stage, the user can start data retrieval through a dedicated ftp interface that directly connects the user to the ATSR Dissemination System. To reduce download time, the user can choose different compression options that are executed 'on-the-fly'. The ATSR NRT WWW server is a totally automated system and was designed to be easily exportable to different platforms and operating systems. It is also independent from the NRT operational environment since communication with the ATSR NRT system is based on an ftp connection, thus making it possible to install one or more ATSR WWW servers at different sites, remotely located from the acquisition facility.

Current Status and Operations

The ATSR NRT system has been providing an operational service to users since mid-July 1999. Any user can access the WWW pages and query the product catalogues. ATSR data download is regulated by ESA data policy for fast-delivery products. To access internal pages, a user obtains a personal account provided by the ESRIN Help

4

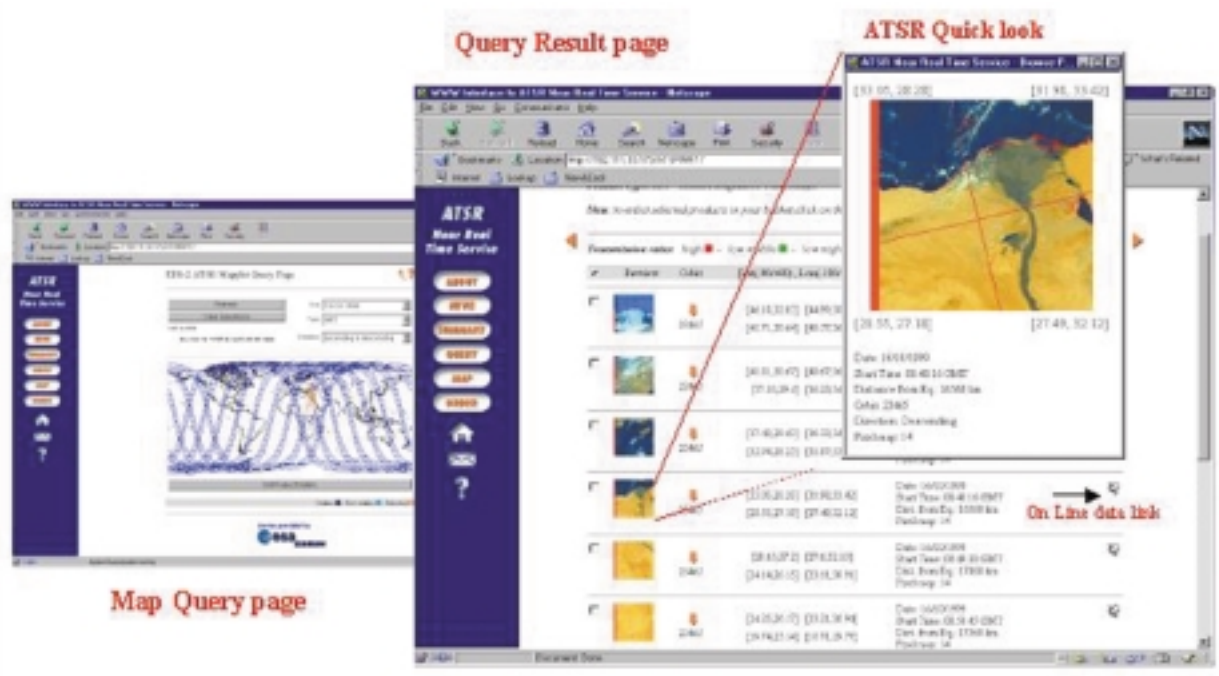

The ATSR NRT WWW interface pages for quering products queries.

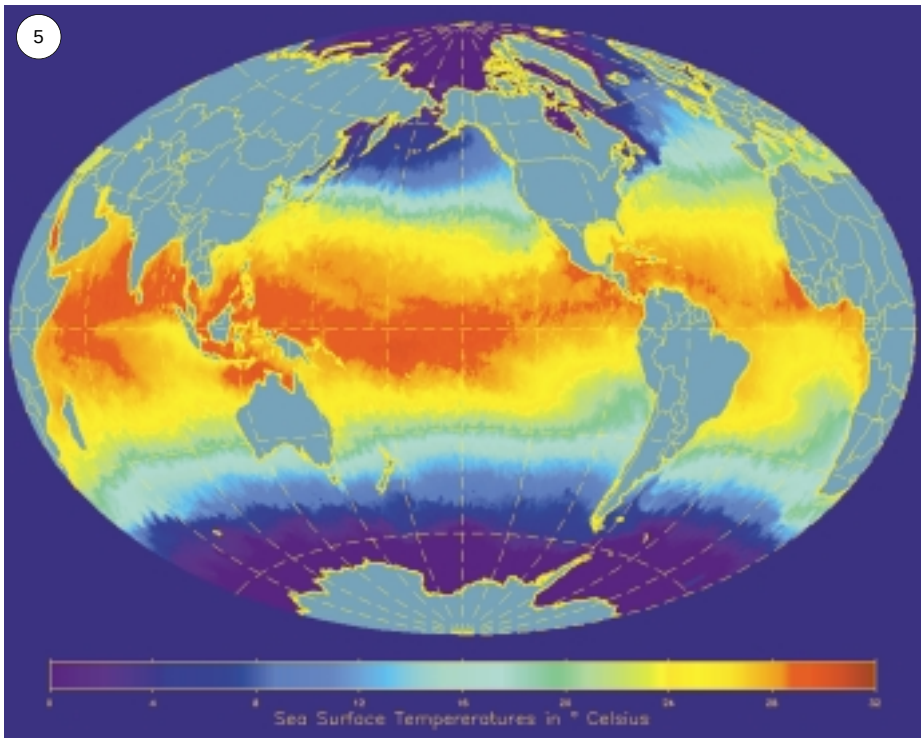

November 1999 image of monthly averaged sea surface temperatures on half-degree latitude/longitude cells.

Desk. Instructions for requesting accounts are provided on the ATSR WWW home page.

The operational scenario is flexible with a number of parameters that can be configured to modify the amount and the type of products available online. Due to acquisition frequency and to consequential time constraints for processing, it is not possible to re-process backlog data. Therefore, all required products have to be planned in advance.

Currently, ATSR GBT and ASST products are systematically generated for all orbital segments acquired, while approximately 10 GSST products are generated for limited sea areas per orbit.

During the first 3 months of operation, approximately 26 Gb of ATSR NRT data were downloaded from the TSS facility by about 50 registered users.

Example of Applications Exploiting ATSR NRT Products

In the short time that the ATSR NRT service has been operational, it has already been used to provide data to projects for monitoring specific environmental events, namely:

- During the summer of 1999, the ATSR Rush Fire products [*Buongiorno et al.*, 1997] were generated in NRT to provide hot spot information for the experimental fire and volcano monitoring campaigns in southern Italy.

- ATSR NRT GBT data will be integrated into operational Boreal Forest Fire survey in northern Europe, currently under development by VTT Automation (F) in the framework of Earth Observation technologies for ESA Decision Support Demonstration (DECIDE) projects (AO/1-3468/98/I-DC).

- A demonstration project set up by ESRIN [*Cardon and Houghton*, 1999] systematically takes all NRT ASST-generated data to provide updated maps (Fig. 5) showing the evolution of ocean temperatures and possible temperature anomalies <(http://odisseo.esrin.esa.it>.

- A global volcano monitoring demonstration project is under development at ESRIN, aimed to provide geophysical parameters for the analysis of volcanic activities in near realtime.

- ATSR data has been retrieved from the realtime service for monitoring the collapse of South Pole ice shelves.

References

Buongiorno, A., Arino, O., Zehner, C., Colagrande & Goryl, P., ERS-2 Monitors Exceptional Fire Event in South-East Asia, EOQ, 56-57, December 1997

Buongiorno, A., The ESA/ESRIN ATSR Browse Generation System (ABS), EOQ, 52, June 1996.

Cardon, K., Houghton, N. & Goryl, P., ATSR Averaged Sea Surface Temperature Services, EOQ, 65, March 1999.

Reports of the International IDNDR Conference on Early Warning Systems for the Reduction of Natural Disasters, EWC'98 Potsdam, Federal Republic of Germany, 7-11 September 1998.

Bailey, P., SADIST-2 v100 Products, ER-TN-RAL-AT-2164, Rutherford Appleton Laboratory, 6 September 1995.

Credits

The ATSR NRT system development was carried out by Kongsberg Spacetec AS under ESA contract (12574/97/I-HE). The WWW user interface for browsing ATSR NRT data was developed by Web Bridges S.r.l. under ESA contract (12974/98/I-DC). The ATSR NRT system operated by the Tromsø Satellite Station.

ATSR Global Averaged Sea Surface Temperature (ASST) Service

Katia Cardon (1), Nigel Houghton (2), Philippe Goryl (3)

(1) SERCO Servizi s.z.l. under contract to ESA/ESRIN, Directorate of Application Programmes
(2)Rutherford Appleton Laboratory (RAL), Space Science Department
Didcot, OX11 0QX Oxfordshire, England
(3) ESA/ESRIN, Directorate of Application Programmes, Earth Observation Applications Department
CP 64, Via Galileo Galilei, 00044 Frascati, Italy

ATSR instruments are designed for the global monitoring of sea surface temperatures using infrared radiation sensors and have been observing the Earth since 1991. Since ATSR-2, which includes 3 additional visible channels, the instrument is also used for vegetation indexes and chlorophyll observation. When ATSR is flying over sea surfaces, the sea surface temperatures are derived from the ATSR measurements [Zavody et al., 1995] and ASST (Averaged Sea Surface Temperature) products are generated. ESA recently developed an additional processing service at Tromsø (N) [Buongiorno et al., 1999], which processes about 10 out of 14 orbits a day and makes the data available in near-realtime.

ATSR-2 Instrument

The ATSR-2 (Along Track Scanning Radiometer) is the most recent operational instrument in the ATSR family, currently flying on ESA's ERS-2 platform since 1995 (see *Mutlow et.al*, this issue).

The information needed for Sea Surface Temperature (SST) retrieval is transmitted from the surface of the Earth to the remote sensing satellite by means of electromagnetic radiation. ATSR is a passive sensor which responds to the radiation that is incident on the instrument. It uses a dual-view, self-calibrating radiometer with 3 visible (V) and near infrared (NIR) channels at 0.55, 0.65 and 0.86 µm (chlorophyll and vegetation index) , 1 infrared (IR) channel at 1.6 µm and 3 thermal infrared (TIR) at 3.7, 10.8 and 12 µm (3.7, 10.8 and 12 µm used for SST retrieval, 1.6 and 3.7 µm used for cloud detection at daytime and nighttime resp.). It also uses a conical scan system providing a double view of the same surface (55° forward and nadir) which allows accurate atmospheric corrections.

The on-board calibration leads to an accuracy of 0.3K of the measurement and a high radiometric sensitivity, signal-to-noise, better than 0.05 in all NIR and IR channels for temperatures higher than 270K. Together with the 12 bits digitalisation enable the detection of fine sea structures and sea temperature variations.

ASST Products

ATSR-2 data are processed with the SADIST-2 processor [*Bailey et al.*, 1995]. The spatially-Averaged Sea Surface Temperature (ASST) product contains temperatures at ten-arcminutes grouped into half-degree cells, using nadir-only and dual-view algorithms. Each half-degree cell contains additional positional and confidence data.

The product consists of a header of fixed length containing orbit parameters, clock calibration parameters and the minimum and maximum temperatures of the instruments detectors, and a number (not fixed) of records. Each record contains the temperature measurements for one half-degree cell.
Each cell consists of:

- the date, latitude and longitude of the cell
- the mean across-track band number
- the mean of nadir-only ten arcminute ASSTs
- 9 nadir-only ASSTs (one for every 10 arcminutes cell)
- the mean of dual-view ten arcminute ASSTs
- 9 dual-view ASSTs (one for every 10 arcminutes cell)
- a confidence word associated with ASST derivation.

Near-Realtime and Offline ASST Products

ATSR-2 data cannot be received directly from the satellite because there is no continuous direct broadcast of data. Instead, the ATSR data collected during each orbit, together with the low bit-rate data from the other sensors on the platform, are stored on an onboard tape recorder for subsequent transmission to the ground. These stored data are then transmitted to the ground during each orbit when the satellite is within the reception range of one of the designated ESA ground stations – Kiruna (S), Maspalomas (ES), Gatineau and Prince Albert (CAN). Kiruna is the main station receiving about 10 of 14 orbits of data collected each day.

The data received at the ground stations are then supplied to the RAL processing facility, where the ASST products are generated. This facility offers an off-line ASST product generation service, which provides the products with a few days delay. Therefore, ESA has developed a near-realtime service which is now in operation at the Tromsø Satellite Station (see *Buongiorno et al.*, this issue).

Near Real Time ASST Products

ASST near-realtime products (products processed at Tromsø) are available through the ASST website at ESRIN, <http://odisseo.esrin.esa.it>. At this

site, you can download ASST products, grouped into one tar file per day (Fig. 1), free of charge. The ASST products remain available at least until RAL has produced its offline products.

Information directly related to the ASST products can be found under 'Instrument Info' and 'Product Info' as well as in the 'Beginner's Guide'. The 'Beginner's Guide', which can be accessed through the home page, provides some basic information on the principals of remotely-sensed sea surface temperatures, a brief description of the ATSR Instrument and its coverage, and the processing chain which generates the final ASST products (Fig. 2).

Furthermore, different kinds of global sea surface temperature maps are available. Firstly, there are the daily updated maps, (available under 'Latest Maps'). These maps show the sea-surface temperature, also with respect to the corresponding monthly mean in 1995 derived from the dual-view data within the product. The values of the maps are updated on a daily basis with the newly available data. No interpolation or any other operation is performed.

1

Homepage of the ASST near-realtime service website at ESRIN.

Another kind of image is available under 'Monthly SST Maps'. These maps represent the sea-surface temperature (or that of the corresponding month in 1995), averaged over a one-month period. Whenever offline ASST products become available at RAL, the maps are replaced with this data. The maps are also available in ASCII format, and occasionally some information about sea-surface temperature related events around the world are included, such as El Niño and its global effects in 1997-1998 (Fig. 3).

The same maps are used in 3-D representations of a part of the Pacific Ocean. In these images, the colour represents the sea surface temperature with respect to the temperature in 1995, and the height is derived from radar altimeter data (Fig. 4). Animations of all maps are available in two sizes under 'Animations'.

2

Two complementary ATSR ASST processing chains, near-realtime and offline (Beginner's Guide) <http://odisseo.esrin.esa.it/asst/>.

ASST Service at RAL

The ASST product generation service at RAL produces the most accurate and complete ASST data set available, generated from the complete set of raw data received from all ground stations using the most accurate set of orbital elements. This is available free of charge via anonymous FTP. It complements the Tromsø near-realtime service that produces ASST products within a short period of time of acquisition, from the 10 of 14 orbits per day available to that receiving station.

Raw data tapes are received at RAL between 2 and 14 days from the date of acquisition. Normally, this data is processed immediately and the generated ASST products are made available via FTP within 10 minutes of generation.

Once all of the data for a particular month has been received and

3

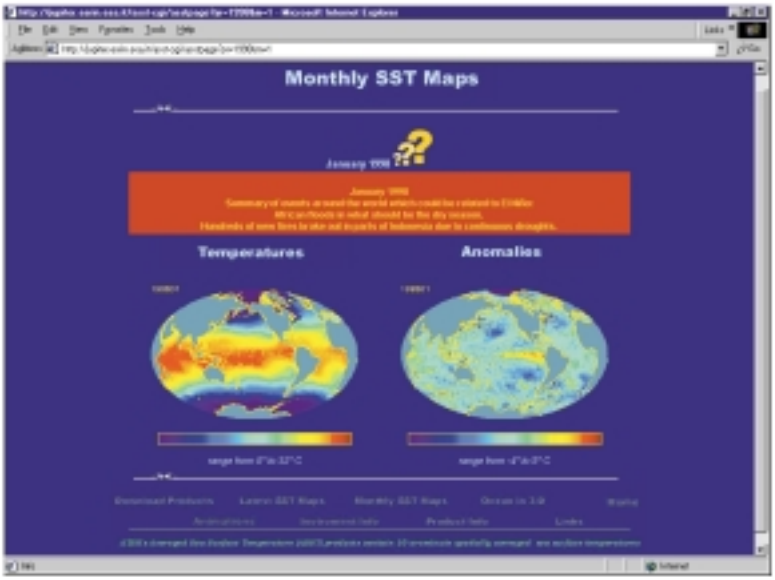

Sea surface temperature and anomaly maps, including additional news related to oceanographic phenomena <http://odisseo.esrin.esa.it/asst/>.

processed, a monthly map of ASST data is produced and made available via the WWW. Additionally, the ASST products themselves are then collected together in one (zipped/compressed) file to allow easy transfer via FTP. The date at which this is available is determined by the date on which the last data for that month is received at RAL, and is typically around the middle of the following month (i.e. January product generation will be completed in the middle of February, etc). An e-mail list is used to inform customers of the completion of processing and the availability of monthly maps. Details of how to join this mailing list and how to transfer ASST products are given on the RAL ATSR WWW page at <http://www.atsr.rl.ac.uk>. This WWW page also contains other valuable information such as latest news, calibration/validation information, detailed product documentation and recent scientific research including development of the algorithm for SST retrieval.

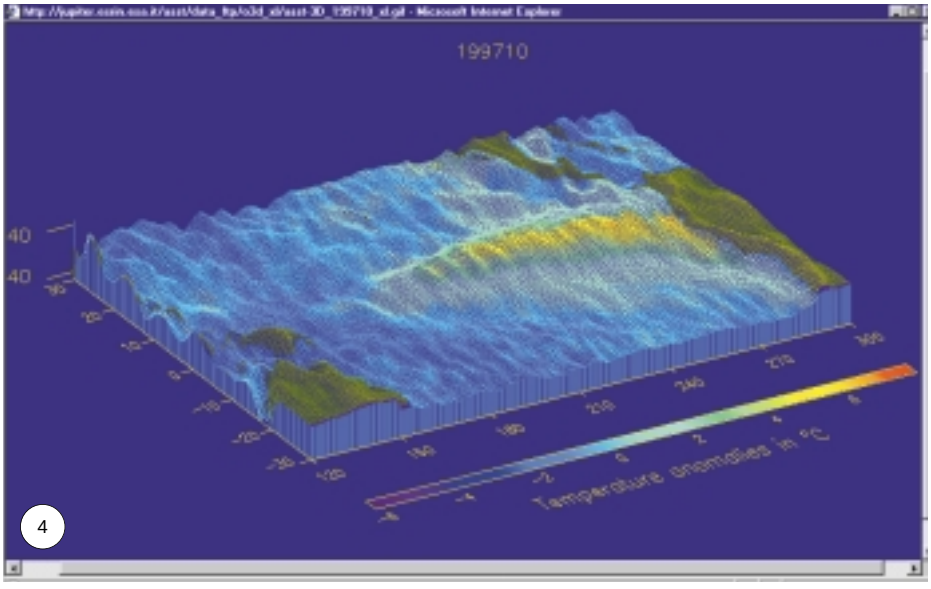

4

Representation of a part of the Pacific Ocean in 3-D, where the colors represent the sea surface temperature and the height is derived from radar altimetre measurements <http://odisseo.esrin.esa.it/asst/>.

In addition to the complete ATSR-2 ASST data set available from this site, the service is being extended to include the whole ATSR-1 ASST data set. This will provide an almost continuous data set for a period of over 8 years. It is hoped that this part of the project will be completed by March 2001.

Whilst the ASST products generated from ATSR data are already of high accuracy, development of the retrieval scheme continues in order to improve on the current products. Traditionally, production of a new data set would require the reprocessing all of the raw data set along with the resulting effort and time delay involved. However, the current method for producing ASST data sets results in another data set of an intermediate product, stored at RAL. This enables a new ASST product derived from updated retrieval schemes to be generated very quickly. A CD containing a new data set will be available sometime in 2000.

Conclusion

Thanks to the installation of an ASST near-realtime service, two complementary data processing chains are now fully operational: this service combined with the offline service, amply fulfil the needs of the user community. The services can be used for the realtime monitoring of oceanographic and climatologic phenomena, such as El Niño and La Niña events.

References

Buongiorno, A., Goryl, P. & Doyle, E., The New ESA/ESRIN ATSR Near-Realtime Service: Development, Operations and Data Distribution, EOQ, 65, March 2000.

Bailey, P., SADIST-2 v200 Products, ER-TN-RAL-AT-2164, Rutherford Appleton Laboratory, 6 September 1995.

Zavody, A.M., Mutlow, C.T. & Llewellyn-Jones, D.T., A radiative transfer scheme for SST retrieval for the ATSR, J.Geophys. Res., 100, 937-952, 1995.

ESA/RAL ATSR Workshop Summary

P. Goryl, A. Buongiorno & G.Kohlhammer

ESA/ESRIN Directorate of Application Programmes, Earth Observation Applications Department
V.Galileo Galilei 00044 Frascati, Italy
E-mail: pgoryl@esa.esrin.it, abuongio@esrin.esa.it, gkohlham@esrin.esa.it

ESA and RAL held a joint International ATSR workshop at ESRIN, Frascati, Italy from 23 to 25 June 1999. The workshop was considered by all participants, as well as by RAL and ESA, to be a very successful meeting, and an important step in increasing the flow of information and contact among ATSR users, ESA and the ATSR project team. The purpose of this workshop was to take stock of the achievements in science and application projects using ATSR data, to introduce new applications, to discuss plans for ENVISAT, and to inform the user community of the status of the ATSR programme.
A total of 36 talks, and 15 posters and demonstrations were presented to some 120 participants in five areas: CAL/VAL & AATSR, Land Applications, Clouds and Aerosol Applications, SST/Climate Monitoring and Oceanography.
A CD-ROM of the proceedings will be available on request from ERS Help Desk (eohelp@esrin.esa.it) later in the year.

CAL/VAL
This session focussed on the validation of ATSR SST using data collected during several ocean campaigns. Preliminary results indicate good coherence between in situ measurements and ATSR data. Various methods were presented to determine skin-bulk temperature differences and support improved validation systems for sea skin temperature retrieval of ATSR, AVHRR and AATSR.

A land surface reflectance validation was also presented based on data collected in four field campaigns. The results show surface reflectance can also be retrieved with a high degree of accuracy from ATSR instrument data.

Both ATSR instruments were deemed to be in very good condition and RAL highlighted the regular generation of calibration information from VISCAL unit data. Calibration coefficients for visible channels, routinely computed, are now available from the RAL website, and RAL has issued detailed information to ensure correct usage <http://www.atsr.rl.ac.uk/>.

AATSR
AATSR data products were presented to the user community, highlighting the changes in format and processing algorithms. A dedicated AATSR working session was also held to discuss future AATSR validation tasks. A recommendation was made in order to coordinate with the Meris Cal/Val team and the NASA funded group.

Land
Eight presentations were given on land applications, demonstrating the suitability of the ATSR for deriving geophysical land parameters. The high-radiometric resolution and the low-noise detectors of the ATSR instrument allow fine distinction of land cover characteristics, making ATSR data suitable for accurate forest/landcover mapping, fire monitoring and detection of burnt areas. A new application for retrieving ice temperature was presented. The synergy between ATSR and other Earth Observation instruments such as SAR, Polder, AVHRR and Landsat was highlighted as being of particular interest in improving analysis of land parameters.

Two papers addressed the potential of the ATSR dual view capability, showing its application in retrieving land surface temperature and in separating atmospheric effects from the land surface reflectance. As use of ATSR dual view for land application depends on a forward view correction for terrain elevation, RAL was asked to provide users with information on topographic correction of ATSR images. Moreover, a good cloud-clearing algorithm over land remains an important issue for all land applications.

Another important issue discussed in this session was the need for a consolidated algorithm to generate future AATSR vegetation products.

Cloud and Aerosol
Cloud and aerosols detection, and cloud cover estimation is always of considerable importance for the analysis of oceanographic processes and for the retrieval of geophysical parameters. This session included the presentation of new algorithms for improved cloud classification with extensive synergistic use of ATSR-GOME data for retrieval of various aerosol types and for assessment of cloud parameters computed by the two instruments. Another significant contri-bution for improving cloud detection is the exploitation of ATSR dual views composed in stereo mode. This promising technique, based on stereo matching, was demonstrated to be suitable for operational processing and allows determination of both cloud top height and cloud coverage from the ATSR data.

Sea Surface Temperature
This session addressed considerations and improved methods for retrieving skin and bulk SST temperatures to achieve the precision necessary for a long-term analysis of climate change. Results were also presented from the comparison between ATSR and AVHRR SST data, with interesting

considerations on the possibility and potential of merging the measurements from the two instruments.

Oceanography
In this session, most papers analysed use of ATSR combined with altimeter data and, in some cases, with other data such as SAR, TOPEX/Poseidon, AVHRR and SeaWiFS. The long-term analysis requirement and the necessity of synergistic use of multiple data types, mean ERS and ENVISAT have signi-ficant potential for improving the understanding of ocean circulation and atmosphere ocean interactions.

Posters and Demonstrations
In the posters and demonstration area, the recent ESA development of a Near-Realtime Service was announced and acquire, process and make available many ATSR products that users can access from a dedicated WWW interface within three hours from acquisition. To ensure maximum area coverage from a single station, the ATSR NRT system has been installed at Tromsø Satellite Station (Norway), which can acquire and process about 10 ERS-2 orbits each day.
As direct demonstration of the potential of ATSR NRT data for the Earth Observation, some specific work on seasonal fire monitoring and ENSO phenomena monitoring were presented here.

Other interesting studies look at the synergy of ATSR and GOME in various application fields. In the demonstration area, flashback imaging of Ontario showed a powerful new PC-based software for the analysis of large data sets, which included a demonstration with ATSR stereo images.

Matra Systèmes & Information presented their new software system, developed under ESA contract, for processing and visualising several different types of EO data. This is particularly suited to exploit synergy between different sensors.

Conclusion
This workshop has demonstrated the considerable potentiality of ATSR for numerous applications: land, ocean, climate, clouds, aerosols and ice. The advantage in using ATSR in synergy with others instruments was highlighted in many presentations. It has been noted that ENVISAT will offer even more opportunities. The dual view capacity is very useful especially for atmospheric applications.

This workshop has led to some recommendations and interrogations: the need to have good operational algorithms for atmospheric correction, cloud clearing and terrain correction over land was stressed. For climate monitoring, high-precision sea surface temperature is recognised as a key parameter and requires longterm series (more than the 15 years of ERS-ENVISAT). Therefore, there is a strong user recommendation to provide an instrument with this capability beyond ENVISAT.

It was agreed that this type of international meeting was found to be extremely useful and should be repeated in the future.

ERS-1 : Nine-Year Success Story Comes to an End

Having given excellent service for nine years, over three times its planned lifetime, the ERS-1 mission was ended on Friday 10 March by a failure in the on-board attitude control system. Since its launch on 17 July 1991, ESA's first sun-synchronous polar-orbiting mission, has made 45 000 orbits, acquiring more than 1.5 million individual Synthetic Aperture Radar (SAR) scenes. ERS-1 SAR images, together with the data from other instruments on board, were delivered to a worldwide community of some 4000 users in science and applications. Surface winds derived from the scatterometer and altimeter have been supplied to meteorological services worldwide since 1991. The duration of the mission has also meant that scientists have already observed several El Nio phenomena through combined observations of surface currents, topography, temperatures and winds. The measurements of sea surface temperatures, critical to the understand-ing of climate change, made by the ERS-1 Along-Track Scanning Radiometer are the most accurate ever from space. All these critical measurements are being continued and enhanced by the current ERS-2 mission.

The most exciting results from the ERS-1 mission have been in the field of SAR interferometry, where for the first time precise topographic information could be routinely produced from space data. The ERS-1 and ERS-2 tandem operations demonstrated this technique for various applications and paved the way for the definition of new dedicated SAR interferometry missions.

ERS-2 (launched in 1995) took over the operational services of ERS-1 in 1996. It too has now exceeded its nominal lifetime and remains in excellent condition. Next year ENVISAT will be launched to continue this series of Earth Observation missions.

For further information please contact:
ESA, Communications Department
Media Relations Office
Tel: +33(0)1.53.69.7155
Fax: +33(0)1.53.69.7690

Towards a Global Burned Surface World Atlas

Isidoro Piccolini (1) and Olivier Arino (2)

(1) SERCO Servizi s.z.l. under contract to ESA/ESRIN, Directorate of Application Programmes
(2) ESA/ESRIN, Directorate of Application Programmes, Earth Observation Applications Department
CP-64, Via Galileo Galilei, 00044 Frascati Italy
Phone: 0039 06 94180564, E-mail: Isidoro.Piccolini@esrin.esa.it, Olivier.Arino@esrin.esa.it

This study demonstrates that burned surfaces can be detected worldwide using remotely sensed data. Due to the good geocation accuracy and radiometry ,the ATSR-2 sensor turned out to be well suited for a global analysis of burned surfaces at a low resolution. Different adaptive algorithms for burned surface detection have been tested on many ecosystems. The estimations obtained were validated using supervised classification on Landsat/TM data. These results will allow the definition of a method for the detection of burned areas from vegetation fire at a global level, allowing the production of a global burned surface atlas.

Introduction

Many vegetation fire events occur around the globe during the year, leading to environmental disasters at different levels: on a regional scale, with the destruction of vegetation reserve and danger for human activities; on a global scale, for the atmospheric emissions that contribute to the greenhouse effect and the rise of the mean temperature of the Earth.

Acknowledging the importance of the problems, many actions have been undertaken at an international level. In the 1997 Kyoto convention, the International Community defined guide lines and rules to assess and restrain the emission of all greenhouse gases. Each member was given the responsibility to “have in place a national system for the estimation of emissions of all greenhouse gases” and “cooperate in scientific and technical research and promote the maintenance and the development of systematic observation systems and development of data archives”.

The CEOS pilot project, Global Observation of Forest Cover (GOFC), was defined with the aim to improve the quality and availability of satellite observation of forest and the information derived from these data. Recently, seeing the preliminary results of burned surface evaluation done using ATSR, GOFC has requested the production of 1-Km resolution regional and global area burned products with this sensor.

Since 1998, via an Announcement of Opportunity (AO-329), ESA promoted a project for the development and test of algorithms with the aim to achieve a global burnt area product using the remotely sensed data from ATSR-2. Partners in this work are the Department of Forestry of the Instituto Superior de Agronomia (DEF/ISA – University of Lisbon), the Global Vegetation Monitoring Unit at Space application Institute (GVM/SAI – JRC) and ESA.

The objective of the study is to design a single algorithm capable of detecting burnt areas from vegetation fires at a global level, across the major biomes. A set of algorithms is under evaluation and test across different ecosystems, in order to identify the strengths and limitations of each method related to the particular vegetation under analysis. These limitations were quantified considering the commission/omission errors and over/under estimation of burnt areas. For ground truth, high-resolution data were used.

Methodology Used for Burned Surface Detection

The main physical variations that occur in a vegetation layer after a fire, which can be detected with remotely sensed data, were quantified with different methods in order to create six different scalar indexes, called K-parameters [*Piccolini and Arino*, 1999]. This results in a decrease in the amount of data to be considered, without any loss of information. In particular, healthy vegetation shows higher reflectance in the range between 0,7 µm and 1,3 µm (NIR) than other natural surfaces. In general, this region of the spectrum contains the most useful information for burned surface detection, thanks to the strong reflectance variation that can be found after a fire occurrence [*Pereira*, 1999].

The second physical characteristic is the increase of temperature that occurs over a burned surface during daytime, due to strong solar irradiance absorption and the absence of evo-transpiration that normally transfers energy to the atmosphere in form of latent heat through water vapour. The presence of ash and carbon constitutes a dry layer that does not allow this cooling process, increasing the surface temperature by 7-8 K [*Lambin and Erlich*, 1996].

Knowing these two characteristics and plotting the graph between reflectance in the NIR (0.87 µm) and brightness temperature in the TIR (11.0 µm), it is possible to identify a geometrical behaviour of the points associated with pixels of burned surface (Fig. 1).

The burned pixels move away from the total distribution, in the upper left direction, independent of the vegetation type or atmospheric status. However, these daily differences determine a variation in the total distribution of the scatterplot and must be taken into account beforehand to define any estimation threshold.

By using an adaptive method, these scalar parameters were decorrelated to the possible daily variations (atmospheric, solar illumination, etc). In particular, the K1 parameter is proportional to the geometrical distance calculated in the previous scatterplot, from the point analysed and the point defined from the mean values of NIR and TIR of the image under analysis. A similar concept was used for the definition of the parameters K2 and K3, using the data in the IR (InfraRed) and the GEMI (Global Environmental Monitoring Index).

The K4, K5 and K6 were defined on temporal analysis of the remotely sensed data. The percentage difference between the NIR value and the mean NIR value in the image were used to create the K4 parameter's image. Using the same concept, the K5 was defined by the difference between brightness temperature at 11 micron and the mean value for the entire image in the same channel. K6 was defined from the spatial feature identified over burn scars. It represents the variance calculated in the red channel for each 3x3 grid centered in the pixel under analysis.

The retrieved images (K-parameter) were elaborated using different rules that allowed the burned/unburned characterisation for each pixel. The tests applied are all adaptive in order to alleviate the artifact due to different viewing geometry, solar illumination or atmospheric conditions.
For K1, K2 and K3 a bayesian method was used in order to decorrelate the final estimation from different vegetation types. In particular, K-parameter data are also calculated from a training set of 10 images of the same vegetation under analysis showing known burned surfaces. The resulting probabilities were used in the bayesian estimator, evaluating the probability P (BS/Kval), that the pixels belong to the burned surface if its K value is at certain level. Finally, these burned surface probability images were compared with a threshold determined on the training set, allowing the definition of a burned surface map derived from each K's method.

A temporal approach has been used to define the rules for K4, K5 and K6 parameters. Considering the time series value for each of these parameters on the same pixels, in order to obtain a temporal behavior filtered from error caused by cloud cover or great daily atmospheric variations, the time series were averaged with a temporal window of six-sample length. The resulting time series appear smoothed, but clearly showed the temporal variations connected with new burned surfaces occurrences. In particular, a decrease in the K4 time series or an increase in the K5 or K6 time series is associated with a permanent variation on the ground, mainly because the vegetation was burned.

Therefore, if the decrease/increase in these time series exceeds a threshold based on the mean time series values, the correspondent pixel is identified as burned surfaces.

West Africa Test Site
A 1000 km2 area was selected to develop and test the method (Fig. 2). This area has three main characteristics:
– a high level of fire activity
– a broad type of vegetation
– a fairly flat region which reduces geolocation error of remotely sensed data.

The period of the year chosen for the study corresponds to a phase of high-level fire activity within the area. From previous studies [*Hao and Liou*, 1994] it was demonstrated that the African continent contributes up to 46% to the total biomass burning in the world. Moreover, occurrences of fires in this continent shows a seasonal activity [*Arino and Rosaz*, 1999] linked to climate variation during the year. The period of the year identified was from January to April 1997, which corresponds to a maximum fire activity period.

The information concerning land cover was extracted from the vegetation map realised in the context of the International Geosphere Biosphere Program (IGBP 1996). The zone under analysis is mainly composed of savan-

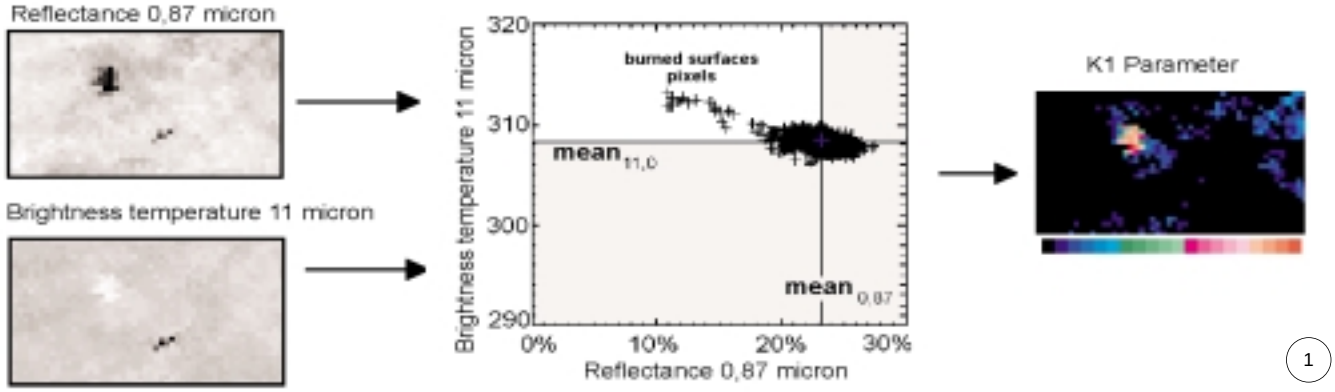

K1 parameter design. The definition of this parameter is based on the geometrical characteristics of the burned surface pixels in the scatterplot between NIR and TIR value. These pixels present low NIR and high TIR values and are mapped away from the classical distribution of the entire image. The distance between normal and burned pixels is quantified in the K1 scalar parameter, using mathematical relations.

nahs (northern central), grassland and cropland (north), woody savannah (southern central), and evergreen broadleaf forest (south).

Preliminary results, subcontinental burned surfaces map in West Africa
The different methodologies were evaluated on the defined zone, estimating the occurrence of the burned areas. To illustrate the distribution of these events from a temporal and spatial point of view, Figure 3 shows the estimation done in this area for three different months during the period under analysis.

Various conclusions can be achieved with this map. Firstly, that the burn occurrences are related to the vegetation area and, in particular, with savannah and woody savannah representing the vegetation in the central part of this region. Secondly, the fire season in Burkina is the earliest in the entire zone. Many burned surfaces were detected in January (green) and a low amount of this is detected in February as well (yellow). Moreover, only few new burned surfaces appeared in February (red). (The opposite situation has been ascertained in Southern Mali and the Ivory Coast, where a large number of burned surfaces were detected in February.)

Validation
Due to the fact that no coherent field data exists, the different procedures were tested on the identified area and validated using nine Landsat/TM images, located on different vegetation zones and on different days (Fig. 4).
The burned surface area was estimated in Landsat/TM by supervised classification (SC), with the maximum likelihood method. In particular, five different classes were identified in the images (burned surfaces, vegetation, river, clouds and cloud shadows) and their spectral signatures in the seven TM channels were collected from a sample set identified by visual inspection.

In order to demonstrate in a visual way the accuracy of this estimation method, RGB composition of Landsat/TM channels, used in different studies for visually discriminate burned surfaces, are shown in Figure 5.

2

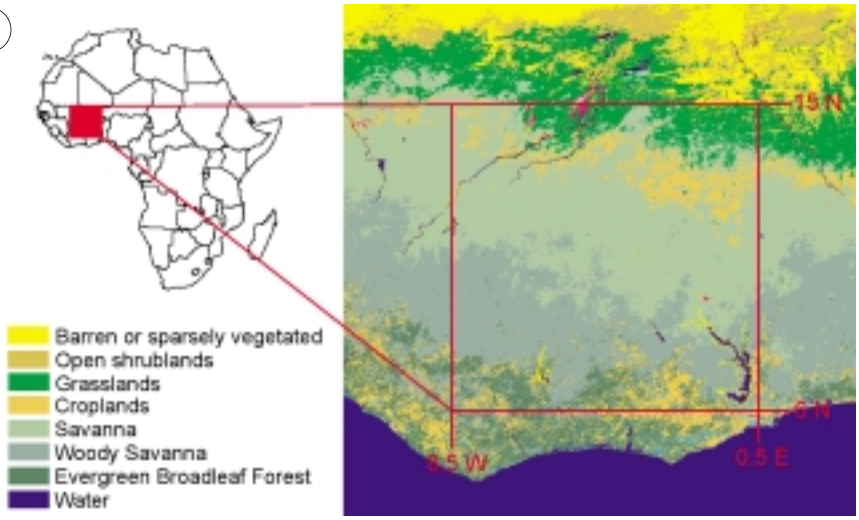

Area under analysis. The different colors show many vegetation types (IGBP 1996) inside the test area of 1000 km2 in West Africa.

In Figure 6, it is possible to note a sample monitoring over the burned area. This large burn scar was found in the savannah using the described techniques and monitored with three samples in order to show the accuracy of the system. As can be seen, a large burned area appears in the second sample. It can be evaluated in high resolution by visual inspection on the NIR channel of Landsat, or by supervised classification on the different channels. Based on ATSR data, the automated method allows a good estimation in low resolution, more suitable for continental or global analysis.

Quantitative validation
To compare the area estimated from the different K-parameters with the one obtained from TM supervised classification, taking into account the different sensor's resolution and geolocation problems, a set of sub-areas were

3

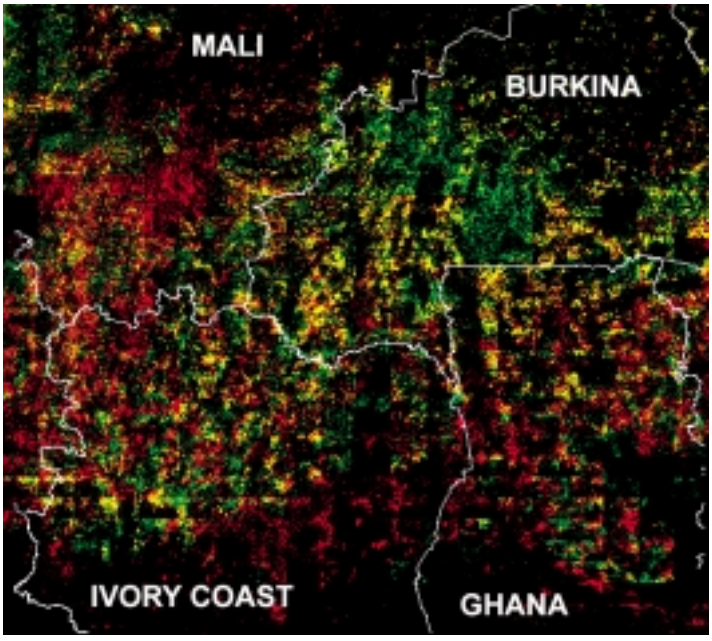

Burned surfaces detected with the K1 parameter in the entire zone under analysis (detection period: green-January, red-February, yellow-both January & February).

4

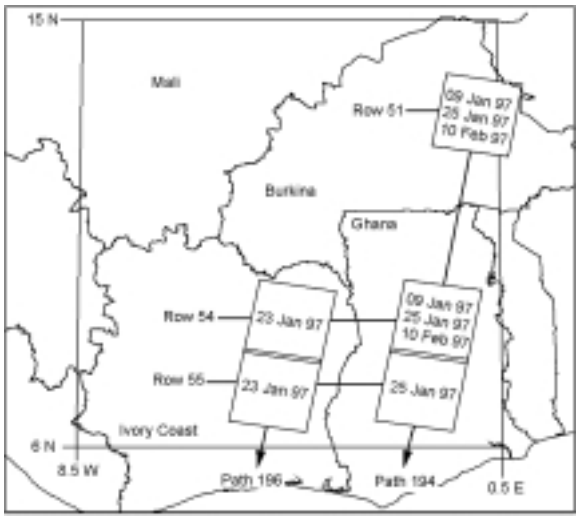

Area under analysis and multi-temporal Landsat/TM coverage. We can see the acquisition date and path/row coordinates of TM images used for the validation.

identified around burn scar occurrences in the supervised classified images. Inside each sub-area, the burned surfaces (in square kilometres) was calculated with the estimations derived from each K-parameter and from the supervised classification. Performing a regression analysis on the retrieved areas, on sparsely burned occurrence areas, the regression coefficient from K1 and K3 estimator are near to one (m_{K1}=1.03, m_{K3}=1.11) and the offsets are also very low (Fig. 7).

Conclusion

The burned areas can be detected using the ATSR-2 data. The physical characteristics of the biomass burned can be detected using the visible, near-infrared and infrared channels. Six algorithms have been developed using adaptive methods.

The first validation studies were performed in West Africa using high-resolution data. The results indicate very good accuracy, particularly con-sidering sparsely burned surfaces for different types of vegetation. Further improvements are expected from the ongoing validation on different biomes.

The perspective is to derive a harmonised global method simple enough to run on 1-km global data sets for several consecutive years, in order to maintain an upgraded archive of burned surface occurrence all over the world.

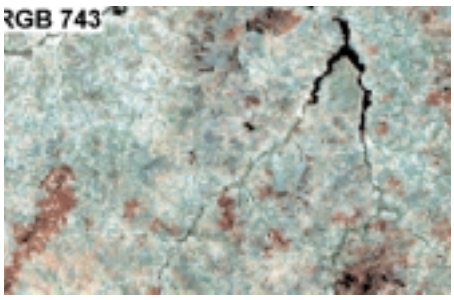

5a

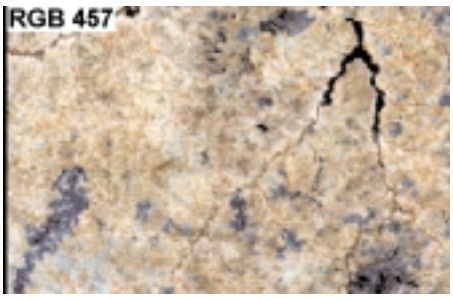

5b

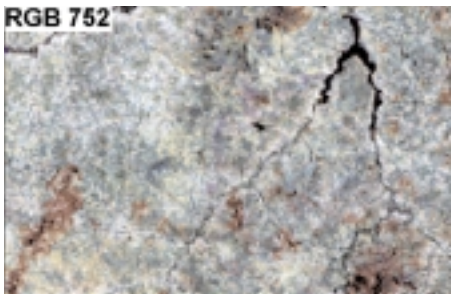

5c

Many studies have been done for burned surface detection using RGB composition on Landsat/TM data. As we can see in these pictures, different RGB compositions allow the identification of this surface by visual inspection. (a) RGB 743 - Pereira J.M.C. et al., (b) RGB 457 - Williams C.M., (c) RGB 752 - Eurimage's analysis, (d) RGB 741 - Koutsias and Karteris 98, (e) RGB 645 - Piccolini 98. Supervised classification (f) allows this evaluation in an automated way and the results are in accordance with previous visual analysis (red-burned surfaces, green-vegetation, black-water).

5d

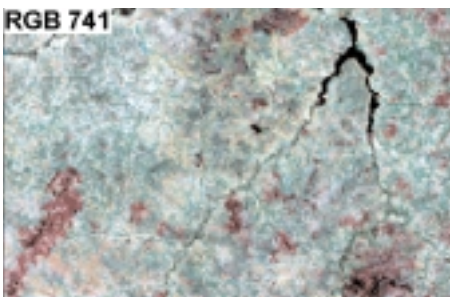

5e

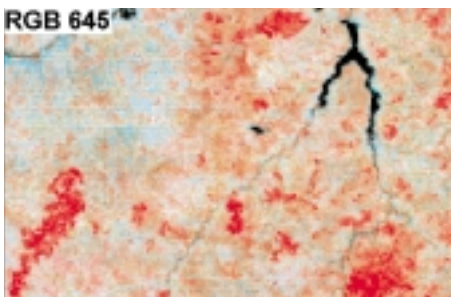

5f

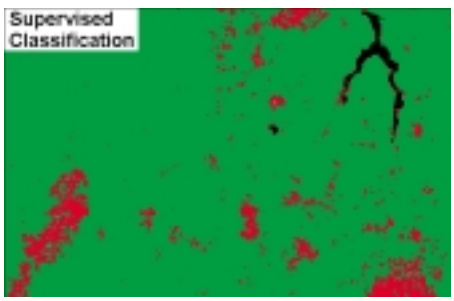

6

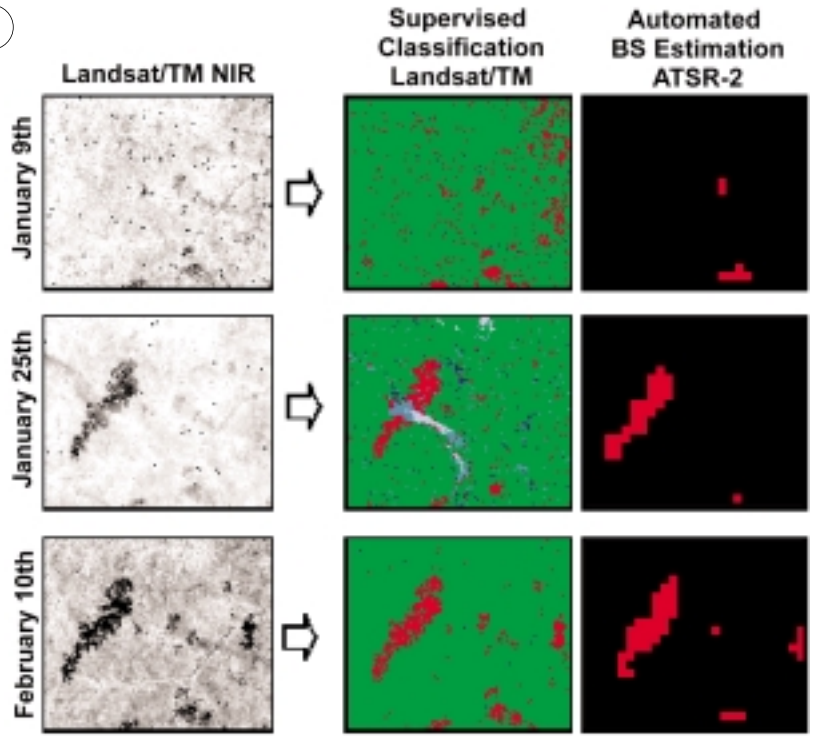

Temporal monitoring of burned areas. A large burned area appears on the second sample. It can be detected in the Landsat NIR image by visual inspection, or with supervised classification on Landsat channels. Based on ATSR data, the automated method allows a good estimation in low resolution, more suitable for continental or global analysis.

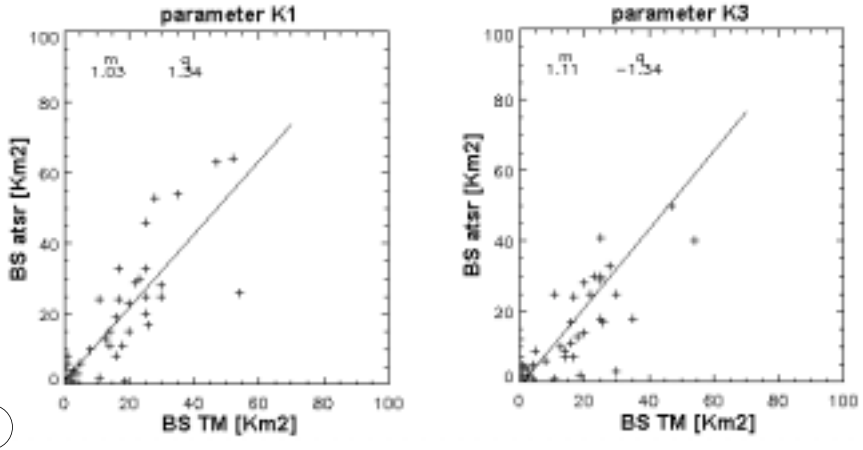

7

Regression analysis between the BS area estimated from the K-parameter and from Landsat supervised classification (zone with sparsely burned surface occurrence). Also represented In the graphs are the regression coefficient m and the offset q.

References

Arino, O. & Rosaz, J., 1997 and 1998 World ATSR Fire Atlas using ERS-2 ATSR-2 Data. Proceedings of the Joint Fire Science Conference, Boise, 15-17 June 1999, 1999.

Hao, W.M. & Liou, M.H., Spatial and temporal distribution of tropical biomass burning. Global biogeochemical cycles, 8 (4) 495-503, 1994.

Koutsias, N. & Karteris, M., Logistic regression modelling of multitemporal Thematic Mapper Data for burned area mapping. International Journal of Remote Sensing, 19, 3499-3514, 1998.

Lambin, E.F., & Erlich, D., The surface temperature-vegetation index space for land cover and land cover change analysis. International Journal of Remote Sensing, 17, 463-487, 1996.

Pereira, M.C., A Comparative Evaluation of NOAA/AVHRR Vegetation Indexes for Burned Surface Detection and Mapping. IEEE Transaction on Geoscience and Remote Sensing, 37, 217-226, 1999.

Piccolini, I., Development and validation of an adaptive algorithm for burn scar detection using ERS/ATSR-2 data. Thesis, Univ. La Sapienza, Rome, 1998.

Piccolini, I., & Arino, O., An adaptive Algorithm for Automatic Burned Surfaces Estimation with ERS-2 ATSR-2 Data. Submitted to International Journal of Remote Sensing, 18.8.1999.

Williams, C.M., Comparison of Supervised and Unsupervised classification of a multispectral TM image. International Journal of Remote Sensing, 19, (18) 3473-3497, 1998.

High-Resolution Aerosol Maps Exploiting the Synergy of ATSR-2 and GOME

Thomas Holzer-Popp, Marion Schroedter and Gerhard Gesell

Deutsches Zentrum für Luft- und Raumfahrt e.V. (DLR) Deutsches Fernerkundungsdatenzentrum (DFD)
Oberpfaffenhofen, D-82234 Weßling, Germany Phone: +49-8153-28-1382, Fax +49-8153-28-1445
E-mail: Thomas.Holzer-Popp@dlr.de, Marion.Schroedter@dlr.de, Gerhard.Gesell@dlr.de www: http://www.dfd.dlr.de

Currently, operational satellite observation of aerosols is limited to either the oceans or over land to high-reaching or UV-absorbing aerosols with reduced horizontal resolution. To overcome these restrictions the new aerosol retrieval method SYNAER (SYNergetic AErosol Retrieval) was developed within the ESA-AO2 project PAGODA (Project for ATSR and GOME Data Application). SYNAER delivers boundary layer aerosol optical thickness (BLAOT) and type over both land and ocean, the latter as BLAOT percentage contribution of 10 representative components from the OPAC (Optical Parameters of Aerosols and Clouds) dataset. The high spatial resolution of ATSR-2 permits cloud detection, BLAOT calculation over automatically selected dark pixels and surface albedo correction for a set of different boundary layer aerosol mixtures. After spatial integration to GOME pixels, these parameters are used to simulate GOME spectra for the same set of different aerosol mixtures. A least square fit of these spectra to the measured spectrum delivers the BLAOT value and – if a uniqueness test is passed – the aerosol mixture. By feedback of the most frequent type of aerosol in GOME pixels within an ATSR-2 frame to the ATSR-2 optical thickness values, high-resolution aerosol maps are produced. Within the ESA-AO3 project PAGODA-2 (Extending the Applicability of New Methods from PAGODA) SYNAER is currently being validated and further extended. First case studies using ground-based sun-photometer measurements of the spectral aerosol optical thickness from NASA's Aerosol Robotic Network (AERONET) show a good agreement.

Introduction

Aerosol particles affect climate directly by interacting with solar and terrestrial radiation and indirectly by their effect on cloud microphysics (aerosols act as cloud condensation nuclei), albedo and precipitation. Tropospheric aerosol forcing is comparable to global net cloud forcing of approximately -1 Wm^{-2} [*Charlson and Heintzenberg*, 1995]. However, on a regional scale the mean direct radiative forcing by aerosols can be as large as -10 Wm-2 for mineral dust over oceans [*Tegen et al.*, 1996]. Anthropogenic changes of the global aerosol distribution may delay or temporarily mask greenhouse warming.

Our understanding of aerosol impact is extending beyond the single use of sulfate aerosol as aerosol representative in climate models as it was handled up to now: it is recognized that smoke aerosol and mineral dust are equally important and may regionally enhance greenhouse warming. For a review of aerosol impact on climate, see *Charlson and Heintzenberg* [1995].

To assess the impact of aerosols on climate there is a growing need for more detailed information on the aerosol spatial distribution and variation together with its composition. More specifically, we need to know aerosol optical thickness (AOT), its absorption and scattering properties, vertical profiles, size distributions and chemical composition.

Currently, there is only a limited capability for aerosol monitoring. Available products are restricted to the oceans based on AVHRR or GOME. Over land, the sensitivity to low level tropospheric aerosols is low except for UV absorbing aerosols. However, the operational TOMS product is limited in horizontal resolution (50 km) and has difficulties with cloud screening due to the pixel size. In the stratosphere, SAGE limb viewing data have been exploited regularly. With the exception of singular case studies only values of the aerosol optical thickness can be derived so far. A detailed summary of the current status and plans on aerosol retrieval can be found in *Kaufman et al.* (1997) and *King et al.* (1999).

In order to overcome restrictions due to current monosensoral methods a new synergetic aerosol retrieval method was developed at the German Remote Sensing Data Center (DFD) of the German Aerospace Center (DLR).

The New Method SYNAER

Aerosol parameters are retrieved with our method SYNAER [*Holzer-Popp et al.*, 1998] from a combination of simultaneous ATSR-2 and GOME measurements. GOME observes near-nadir reflection in the range from 240 nm to 790 nm with a spectral resolution of 0.2 nm to 0.4 nm and a pixel size of 320 x 40 km^2 or 80 x 40 km^2. The high spectral resolution of GOME supplements, ideally, the high spatial resolution of ATSR-2.

First of all, cloud detection is performed for all ATSR-2 pixels. Boundary layer aerosol optical thickness (BLAOT) values are derived from automatically selected dark ATSR-2 nadir pixels (dark forest, water bodies) for which the surface albedo can be estimated with good accuracy. Using the atmospheric

1

Flow chart of the major steps in the SYNAER retrieval method.

correction scheme EXACT [*Popp*, 1995] which has been validated with Landsat-TM and NOAA-AVHRR data, BLAOT can be estimated for the dark fields and interpolated to all cloudfree ATSR-2 nadir pixels. Then the surface albedo values for the 3 wavelengths 560 nm, 670 nm and 870 nm are obtained for all pixels. The ATSR-2 derived data are colocated to GOME pixels and interpolated spectrally. Using the ATSR-2 calculated values of optical thickness and surface albedo, GOME spectra for different mixtures are simulated at 10 selected wavelengths. A least square fit of the simulations to the measured GOME spectrum selects the most plausible type of aerosol and its corresponding BLAOT value in a GOME pixel. Finally, an ambiguity test is applied. Figure 1 gives an overview of SYNAER.

Cloud Detection

Accurate cloud detection is an important prerequisite for aerosol retrieval. The well-established APOLLO (AVHRR Processing Scheme over Clouds, Land and Ocean) [*Gesell,* 1989; *Kriebel et al.*, 1989] software was adapted to ATSR-2 data. Five ATSR-2 channels, which are equivalent to the AVHHR spectral bands, are used for cloud detection. A number of threshold tests are applied to differentiate types of clouds. APOLLO yields cloud fraction, 4 cloud layers and cloud optical parameters. A typical cloud mask and the corresponding ATSR-2 nadir view as RGB image is shown in Figure 2. High clouds are marked in blue, medium layer clouds in green, and low clouds in yellow. Partly cloudy pixels occur in white. Snow and cloudy pixels can be separated by the APOLLO scheme. Few errors occur along the coastline due to lack in geolocation mapping to a land-sea mask. Since snow pixels cannot be used for aerosol retrieval, they are taken into the cloud mask as white pixels.

Dark Pixel Detection

Dark land ATSR-2 pixels are selected on the basis of the 1.6 mm channel and the reflected contribution to the 3.8 mm channel. As the aerosol effect at this wavelength can be neglected for most aerosol types, all cloud/snowfree pixels with a 1.6 mm reflectance below a given threshold are selected. To reject wet bare soil pixels which are also dark in the 1.6 mm channel but brighter in the visible, the normalized differential vegetation index (NDVI) must be larger than a preset minimum value. For the

RGB image (channels at 670 nm in red, 870 nm in green, 12 mm in blue) of ATSR-2 nadir view and snow/cloud mask derived from the APOLLO algorithm for orbit 12129, frame 2655, 15 August 1997 in northern Italy/the Alps. Clouds in different heights are represented with different colours: high clouds in blue, medium-layer clouds in green, and low clouds in yellow. Snow and partly cloudy pixels are marked as white pixels.

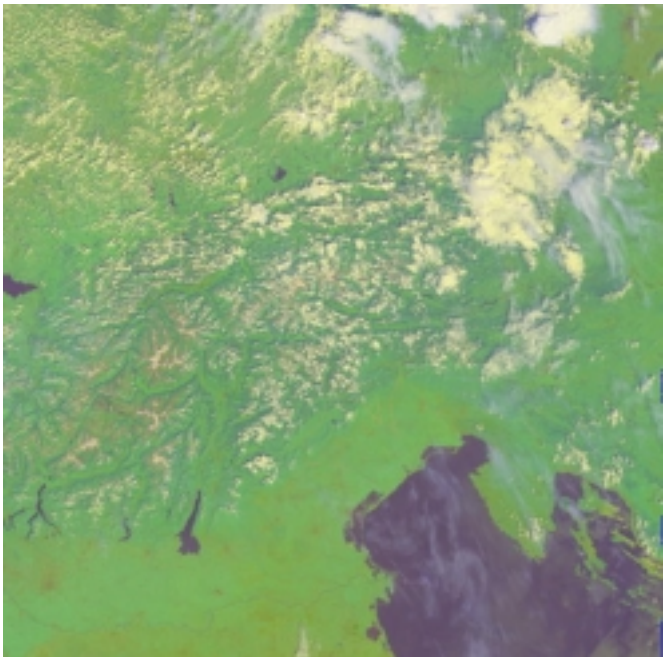

2

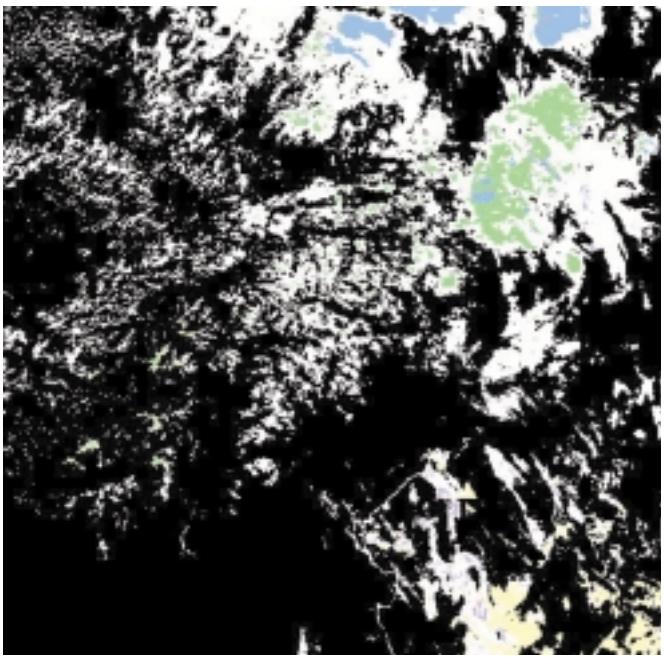

pixels selected through this scheme, the dark field albedo values at 560 nm and 670 nm can then be estimated from the 1.6 mm reflectance by application of a conversion factor. Kaufman et al. (1997) suggest a similiar selection scheme based on the 2.1 mm and 3.8 mm channels of the MODIS sensor onboard the EOS-A platform. Water pixels are exploited only over deep oceans with a fixed albedo.

The accuracy of the retrieved spectral optical thickness values depends highly on the exact knowledge of the surface albedo of the dark fields and decreases with increasing surface albedo. The BLAOT retrieval, based on dark field selection and estimation of their surface albedo values from the 1.6 mm and 3.8 mm channels, shows a significant scatter in the retrieved values of neighbouring pixels. Therefore, a minimum number of adjacent pixels must be exploited to allow for an appropriate averaging. In areas with sparse dark fields, singularities must be rejected. To overcome these difficulties, dark fields are grouped into 4 different classes with increasing surface albedo, i.e. decreasing retrieval accuracy. For boxes of 25x25 ATSR-2 pixels, only dark pixels of the lowest available, i. e. most accurate category, are exploited. Furthermore, pixels are rejected if their retrieved values differ by more than the local variance from the average of their neighbourhood. The range for this variance test is increased stepwise until a minimum pixel number guarantees statistical significance. The details of the dark field selection and characterization are currently under review and will be improved and further validated.

Aerosol Retrieval

Aerosol optical thickness and surface albedo values are derived for 40 boundary-layer aerosol mixtures (Table 1) because the retrieved values depend strongly on the aerosol type. An external mixing approach is used in the boundary layer which allows for the mixing of arbitrary aerosol types from a set of 10 basic components. The following components from the OPAC (Optical properties of aerosols and clouds) database [*Hess et al*., 1998] are used:

– watersoluble (waso): sulfates, nitrates, other organic water soluble substances
– water insoluble (inso): soil particles, water insoluble organic material
– sea salt accumulation mode (ssam): particles with particle distribution mode radius 0.2 µm
– sea salt coarse mode (sscm): particles with particle distribution mode radius 1.75 µm
– soot (soot): absorbing black carbon
– mineral transported (mitr): desert dust transported over long distances.

Tropospheric and stratospheric aerosol optical thickness is set to 0.02 and 0.01, respectively [*World Climate Program*, 1986]. For humidity dependent components, two models with 50% and 80% relative humidity have been included. The same set of 40 mixtures is used in the ATSR-2 BLAOT and albedo retrieval and the GOME simulations.

Aerosol mixes used in SYNAER as external mixes from 6 basic components: watersoluble (waso), water insoluble (inso), sea salt accumulation (ssam) and coarse (sscm) mode, soot, and mineral transported (mitr). Additionally, height of aerosol layer and humidity are given for each mix.

Table 1

				component contributions [%]					
No.	Name	humidity	height	WASO	INSO	SSAM	SSCM	SOOT	MITR
1	Pure Watersoluble	50%	2 km	100					
2	Continental I	50%	2 km	95	5				
3	Continental II	50%	2 km	90	10				
4	Continental III	50%	2 km	85	15				
5	Maritime I	50%	2 km	30		70			
6	Maritime II	50%	2 km	30		65	5		
7	Maritime III	50%	2 km	15		85			
8	Maritime IV	50%	2 km	15		75	10		
9	Polluted Watersoluble I	50%	2 km	90				10	
10	Polluted Watersoluble II	50%	2 km	80				20	
11	Polluted Continental I	50%	2 km	80	10			10	
12	Polluted Continental II	50%	2 km	70	10			20	
13	Polluted Maritime I	50%	2 km	40		45	5	10	
14	Polluted Maritime II	50%	2 km	30		40	10	20	
15	Desert Outbreak I	50%	4 km	75					25
16	Desert Outbreak II	50%	4 km	50					50
17	Desert Outbreak III	50%	4 km	25					75
18	Biomass Burning I	50%	3 km	85				15	
19	Biomass Burning II	50%	3 km	70				30	
20	Biomass Burning III	50%	3 km	55				45	
21-40	humid version (= 1-20)	80%	all 40 mixes: tropospheric aerosol optical thickness 0.02 stratospheric aerosol optical thickness 0.01						

3

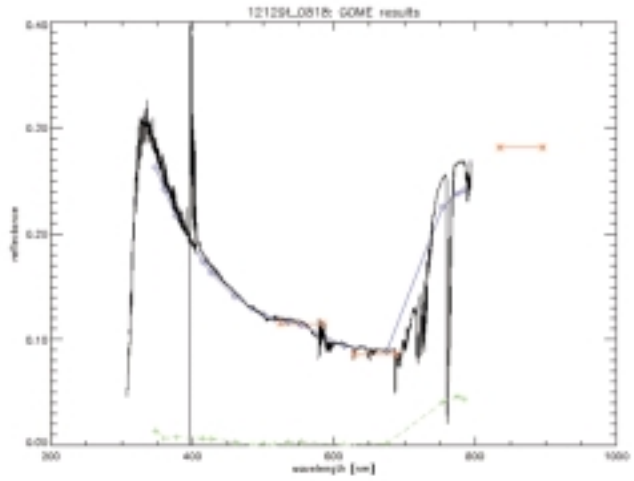

Example GOME spectrum over land with 6% cloud fraction: The GOME spectrum is given in black, the best fitted simulation in blue and the difference in light blue green Additionally, ATSR-2 wavelengths at 560, 670 and 870 nm are plotted in red.

4

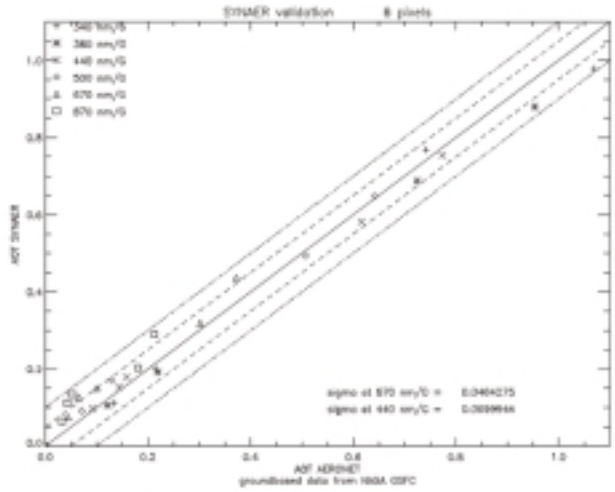

First validation results: Comparison of spectral aerosol optical thickness (AOT) retrieved with SYNAER to AOT measured by AERONET ground stations. Different wavelengths are marked with different symbols. AERONET data were acquired through the AERONET website of NASA-GSFC <http://aeronet.gsfc.nasa.gov:8080>.

All radiative transfer calculations are conducted with an iterative code (successive orders of scattering, SOS) [*Nagel et al.*, 1978] which includes full multiple scattering. For a fast application, pre-calculated radiative transfer tables are used. Figure 3 shows a typical GOME spectrum over land for a low cloud fraction (6%) in black, the best fitted simulation spectrum in blue and the differences of both in green.

Additionally, ATSR-2 wavelengths at 560, 670 and 870 nm are plotted in red. As the simulation often does not fit in the vegetation peak above 700 nm these wavelengths are not exploited for the retrieval.

Within the ERS-AO3 project PAGODA-2 (Extending the Applicability of New Methods from the Project for ATSR and GOME Data Application), we are currently further improving and validating the aerosol retrieval method. Furthermore, we will investigate the possibilities for aerosol retrieval from partly cloudy GOME pixels in order to assess the interaction between clouds and aerosols directly. The basic idea is to look inside large GOME pixels with the high ATSR-2 resolution and to use APOLLO-derived cloud parameters on the ATSR-2 grid to characterise the cloud influence as it is seen by GOME with high accuracy.

SYNAER and ENVISAT

SYNAER will be adapted to AATSR and SCIAMACHY onboard ENVISAT-1 (launch planned June 2001) and applied within the accepted ENVISAT-AO proposal SENECA (Synergetic ENVISAT Data Exploitation for Cloud, Aerosol and Ozone Retrieval). SCIAMACHY has a wider spectral range (up to 2400 nm, GOME up to 790 nm) which enables a better investigation of the aerosol type, especially for large particles, and the additional limb viewing geometry for stratospheric aerosol retrieval. Both instruments offer an improved data transmission rate and allow small SCIAMACHY pixels throughout the entire mission and orbitwise AATSR data.

First Validation Results

For the first case studies, ground-based measurements taken by the AERONET (AErosol RObotic NETwork) stations were used. The objective of AERONET [*Holben et al.*, 1998] is to monitor aero-sols using ground-based spectral radio-meters and validate aerosol retrieval results from satellites like ENVISAT, TERRA and ADEOS-2. The measurements are available to the public from NASA at <http://aeronet.gsfc.nasa.gov:8080>. AERONET provides spectral aerosol optical thickness (AOT) values and aerosol size distributions worldwide.

So far, about 2500 GOME pixels were analysed, but only 66 pixels include ground stations inside the pixel boundaries. Additional criteria for validation pixels (cloudfree ground-based measurements, less than 15% cloud coverage inside the GOME pixel, a maximum of 15 minutes difference between ground measurement and satellite overpass) left six pixels with ground measurements of spectral aerosol optical thickness. All cases are driven by land-based dark fields, 80x40 km2 in size, and a cloud fraction inside the GOME pixel up to 15.4 % (Table 2). Figure 4 shows the retrieved AOT values at 6 wavelengths against the AERONET measurements. A good agreement with errors less than 0.1 for the AOT values can be seen.

High-Resolution Aerosol Maps

High-spatial resolution of aerosol optical thickness is provided by ATSR-2 while the aerosol-type information is derived from GOME measurements. Combining both, as a first and preliminary result, a high-resolution aerosol map for the period 1-3 September 1995 was creat-

Table 2

pixel	1	2	3	4	5	6
date	15/8/97	5/10/97	15/11/97	4/1/98	14/7/98	15/8/98
UTC	9:39	9:36	10:24	15:57	14:28	10:44
latitude	45:18N	45:18N	45:48N	39:00N	16:00S	49:20N
longitude	12:30E	12:30E	8:37E	76:54W	62:01W	7:36E
altitude	10m	10m	235m	50m	500m	~300m
orbit	12129	12859	13446	14165	16898	17354
number	818	589	419	446	1596	767
location	Venice	Venice	Ispra	GSFC	Concepcion	Lindenberg
country	Italy	Italy	Italy	USA	Bolivia	Germany
clouds	5.4%	11.4%	6.1%	15.4%	0.0%	0.0%
author	GZ	GZ	GZ	BH	BH	LACE

Specifications of validation pixels (data courtesy: GZ=Giuseppe Zibordi/JRC, BH=Brent Holben/NASA-GSFC)

ed (Fig. 5) using only daytime ERS-2 orbits. Cloudy areas are masked in white. Interesting features are local maxima of aerosol optical thickness in urban areas such as Paris, northern Italy and Thessaloniki. Lower values over the Alps occur as expected. Over northern Germany, a band of higher optical thickness occurs that might also be a cloud detection error. This is under further investigation.

As a weakness, stepwise transitions between ATSR-2 frames can be seen. This has two reasons: the exploited GOME scan mode has a swath width of 240 km and does not cover the whole ATSR-2 frame. Therefore, the most frequent aerosol type of all GOME pixels inside an ATSR-2 frame was chosen as the aerosol type representative for the whole frame. Using this aerosol type, the aerosol optical thickness (AOT) was calculated for the whole frame and is shown on the map. Additionally, the dark field selection is handled framewise (512x512 km2) and, therefore, border effects might contribute to these edges. In the future, use of SYNAER for SCIAMACHY and AATSR results from both sensors will cover the same area and AATSR data will be handled orbitwise. Therefore, we expect that these edges will vanish.

Conclusions

– A new, unsupervised retrieval method SYNAER for aerosol optical thickness and type in the boundary layer over cloudfree land and oceans from GOME and ATSR-2 data was delevoped and applied.

– Nadir and forward ATSR reflectances were used but forward reflectances seem to be uneligible for our aerosol retrieval scheme. Misregistrations between nadir and forward view in the gridded data product and, therefore, physical information content of different air masses seem to be the reason.

– A first case study validation showed good agreement of retrieved spectral aerosol optical thickness values to ground-based sun-photometer meas urements (error below 0.1 at 340, 380, 440, 500, 670 and 870 nm). Due to a very small number of exploitable ground measurements, only six case studies could be per formed so far. During the last months, the AERONET database was remark ably completed and, therefore, the availability of ground measurements has been improved. Therefore, we are working on further validation.

– Within the setup of a processor for atmospheric value added products, DFD will operationalise the SYNAER method for further use of SCIA MACHY/AATSR, MODIS and GOME-2/AVHRR data. Beside spectral improvements these instruments will provide a better spatial and temporal coverage.

– Our aim is to contribute a satellite-based climatology of tropospheric aerosols from 10 years of ERS-2 and ENVISAT data (July 1995 to June 2005) to improve the understanding of the global temporal-spatial distribution of aerosol loading and its

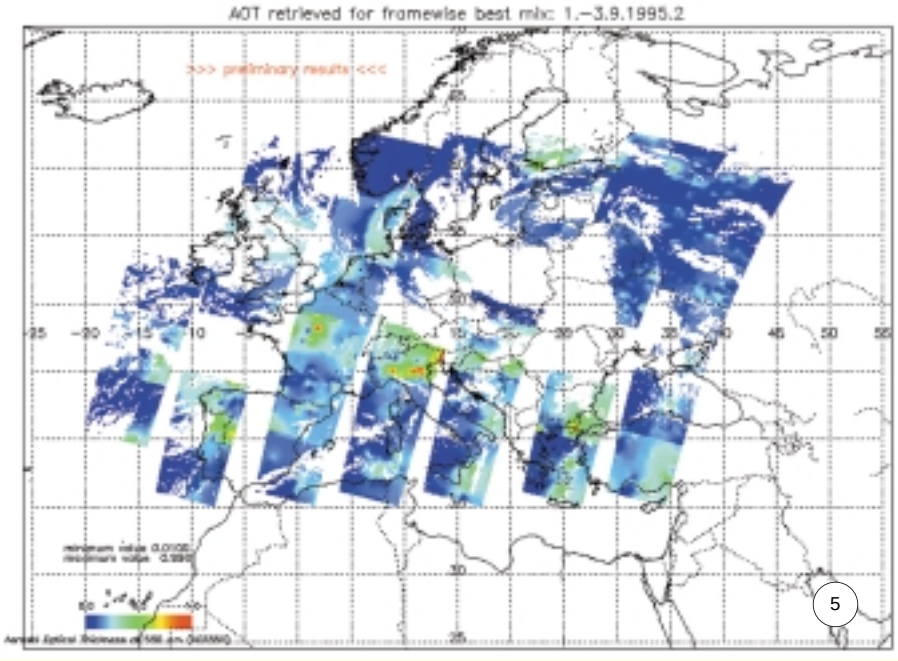

High-resolution aerosol map over Europe Aerosol optical thickness for all daytime ATSR-2 frames acquired over Europe during the period 1-3 September 1995 with 1-km horizontal resolution. Cloud covered pixels are left blank.

major components. The direct implementation of the SYNAER resulting climatology dataset in the global circulation model ECHAM [*Röckner et al.*, 1992] is prepared. Our dataset follows the characteristics of the ground-based dataset GADS (Global Aerosol Data Set) [*Köpke et al.*, 1997] which is currently under implementation in ECHAM.

– Exploiting the synergy of simultane ous measurements of the spectrometer GOME and the radiometer ATSR-2 enables the derivation of high-resolution aerosol optical thickness maps over land. The retrieval process takes care of the variation in the signal due to different aerosol types. These maps (after their improvement and adaption to ENVISAT and MODIS) will be useful for potential customers in local authorities, pollution networks and health services which monitor air pollution caused by particulate matter.

Acknowledgements
The results presented were achieved within the ESA-AO projects PAGODA (AO2.D107-1) and PAGODA-2 (AO3.218) through which the input data (GOME and ATSR-2) were acquired. Our thanks go to G. Zibordi/JRC and Brent Holben/NASA-GSFC for providing AERONET validation data from the Venice, Ispra, Goddard Space Flight Center and Concepcion stations. We thank Peter Wendling/DLR-IPA for the provision of airborne LIDAR measurements from the LACE campaign.

References

Charlson, R. J. & Heintzenberg, J. (Eds.), Dahlem Workshop Report on Aerosol Forcing of Climate, 416 pp., John Wiley, New York, 1995.

Gesell, G., An Algorithm for Snow and Ice Detection using AVHRR data: An Extension to the APOLLO Software Package, Int. J. Rem. Sens., 10, 897-905, 1989.

Hess, M., Köpke, P. & Schult, I., Optical Properties of Aerosols and Clouds: The Software package OPAC, Bull. Am. Met. Soc., 79, 831-844, 1998.

Holben, B. N., Eck, T. F., Slutsker, I., Tanre, D., Buis, J. P., Setzer, A., Vermote, E., Reagan, J. A., Kaufman, Y. J., Nakajima, T., Lavenu, F., Iankowiak, I. & Smirnov, A., AERONET - A Federated Instrument Network and Data Archive for Aerosol Characterization, Rem. Sens. Environ., 66, 1-16, 1998.

Holzer-Popp, Th., Kriebel, Th., Böttger, U., Dameris, M., Gesell, G., König, Th., Meerkötter, R., Rother, T. & Schroedter, M., PAGODA final report, Schriften des Deutschen Fernerkundungsdatenzentrums Nr.1, DLR, Oberpfaffenhofen, 1998.

Kaufman, Y. J., Tanre, D., Gordon, H. R., Nakajima, T., Lenoble, J., Frouin, R., Grassl, H., Herman, B. M., King, M. D. & Teillet, P. M., Passive remote sensing of tropospheric aerosol and atmospheric correction for the aerosol effect, J. Geophys. Res., 102, 16815-16830, 1997.

Kaufman, Y. J., Tanre, D., Remer, L. A., Vermote, E. F., Chu, A. & Holben, B. N., Operational remote sensing of tropospheric aerosol over land from EOS moderate resolution imaging spectrometer, J. Geophys. Res., 102, 17051-17067, 1997.

King, M.D., Kaufmann, Y.J., Tanre, D. & Nakajima, T., Remote Sensing of Tropospheric Aerosols from Space: Past, Present, and Future, Bull. Of the Americ. Meteorolog. Society, Vol. 80, No. 11, 1999.

Köpke P., Hess, M., Schult, I. & Shettle, E. P., Global Aerosol Data Set, Max-Planck-Institut für Meteorologie, Report No. 243, 1997.

Kriebel, K. T., Saunders, R. W. &, Gesell, G., Optical Properties of Clouds Derived from Fully Cloudy AVHRR pixels, Beitr. Phys. Atmos., 62, 165-171, 1989.

Nagel, M. R., Quenzel, H., Kweta, W. & Wendling, P., Daylight Illumination-Color-Contrast-Tables, New York, Academic Press, 1978.

Popp, Th., Correcting atmospheric masking to retrieve the spectral albedo of land surfaces from satellite, Int. J. Rem Sens., 16, 3483-3508, 1995.

Röckner, E., Arpe K., Bengtsson, L., Brinkop, S., Dümenil, L., Esch, M., Kirk, E., Lunkeit, F., Ponater, M., Rockel, B., Sausen, R., Schlese, U., Schubert, S. & Windelband, M., Simulation of the present-day climate with the ECHAM model: Impact of model physics and resolution. Max-Planck-Institut für Meteorologie, Report No. 93, 171pp, 1992.

Tegen I., Lacis A.A. & Fung I., The influence on climate forcing of mineral aerosols from disturbed soils, Nature, 380, 419-422, 1996.

World Climate Program (WCP), A Preliminary Cloudless Standard Atmosphere for Radiation Computation, WCP-112, WMO/TD No. 24, Boulder, 1986

EO Announcement

Several EO applications in urbanism have been developed as part of an Agency General Study contract ‘Demonstration of potential value of ESA Earth Observation Data and Products: End to End Demonstrator: Mega Cities’ and can be visited at <http://earth.esa.int/mcities/>.

The corresponding CD-ROM can be ordered at eohelp@esrin.esa.it. The project was developed by an European consortium lead by SCOT.

Comparison of Cloud Retrievals from GOME and ATSR-2

R.B.A. Koelemeijer & P. Stammes

Royal Netherlands Meteorological Institute (KNMI)
P.O. Box 201, 3730 AE De Bilt, The Netherlands

We compare two independent methods to derive cloud fraction and cloud top pressure from two instruments onboard the ERS-2, namely GOME and ATSR-2. The GOME instrument is a UV/VIS spectrometer measuring the Earth's spectral reflectivity with a resolution of 0.2-0.4 nm. The GOME pixel size is 40x80 km2 for the data presented here. The ATSR-2 is a 7-channel imaging radiometer with a pixel size of 1x1 km2. Our algorithm for GOME, called FRESCO (Fast Retrieval Scheme for Clouds from the Oxygen A-band), makes use of the GOME spectral reflectivity measurements between 758-778 nm (covering the oxygen A-band) to derive cloud fraction and cloud top pressure. Our algorithm for ATSR-2 makes use of the shortwave channels to derive cloud fraction, and of the thermal infrared channels to derive cloud top pressure. The ATSR-2 thermal infrared brightness temperature measurements are converted to cloud top pressures using analysed ECMWF temperature profiles. Generally, the results from GOME and ATSR-2 agree reasonably well. Our FRESCO method is now applied globally to derive cloud fractions and cloud top pressures in near-realtime.

Introduction

Cloud feedbacks form one of the largest uncertainties in global circulation model (GCM) predictions of future climate [*Cess et al.*, 1990]. Therefore, global satellite measurements of cloud parameters are needed to validate GCM simulations of present day climate, and to improve parametrisations of clouds in such models. However, cloud parameters retrieved from satellite measurements must be validated using in-situ measurements, or using independent satellite-derived cloud parameters. The aim of this paper is to present a comparison between independent retrievals of cloud fraction and cloud top pressure from GOME and ATSR-2 data. Because clouds are variable in space and time, collocation is required when comparing different cloud retrieval techniques. The GOME and ATSR-2 instruments offer a unique possibility for such a comparison, as they measure the same atmospheric volume at the same time.

Data Selection

The GOME and ATSR-2 data were acquired on 23 July 1995, between 11:46 and 11:54 UT, and are part of ERS-2 orbit 1337. The considered area is 3500 km long, spanning 7 ATSR-2 images from 74o -52o N. One of these images is depicted in Figure 1, showing

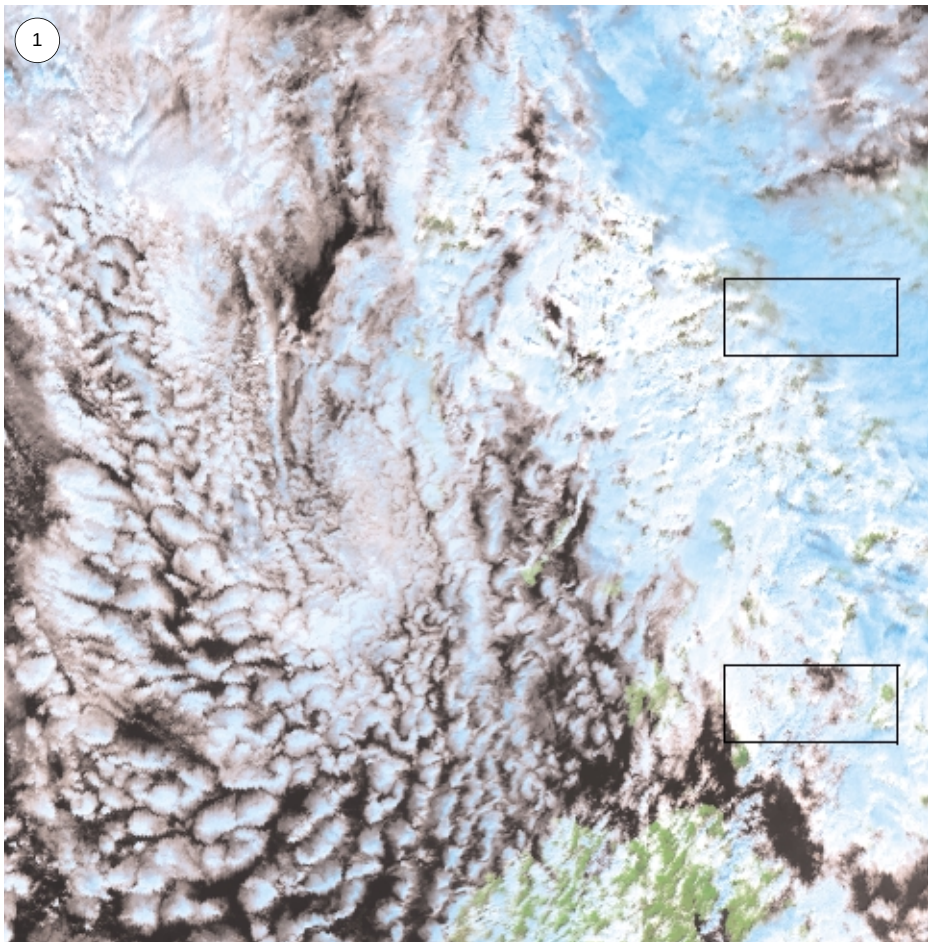

Colour composite of ATSR-2 measurements of clouds over Scotland, Ireland, and the Atlantic Ocean, on 23 July 1995, 11:51 UT. The image is between 55-59o N. The two selected areas indicate the location of the GOME spectra of the high cloud (upper area) and the low cloud (lower area), shown in Figures. 2 and 3.

clouds over Scotland, Ireland, and the Atlantic Ocean. The image is a colour composite of the 0.66mm channel (blue), 0.87mm channel (green), and 1.6mm channel (red). Ice clouds absorb stronger at 1.6mm than water clouds, due to the difference in refractive index and particle size [*Knap et al.*, 1999]. Therefore, ice clouds show up in blue in this image. Scotland is covered by clouds originating from a cold front, pertaining to a low pressure area with its centre north of Scotland.

In the image, two areas are marked: the upper is mainly over high-altitude ice clouds, and the lower one is mainly over low-altitude water clouds. The GOME spectral reflectivity measurements of these two areas are shown in Figure 2. Clearly, clouds themselves are white in the spectral region between 300-800 nm. The sharp decrease in reflectivity below 330 nm is due to absorption by ozone in the Hartley-Huggins bands, whereas the broad, but weaker, decrease in reflectivity between 500 and 700 nm is due to the Chappuis-band of ozone. Other apparent absorbers are water vapour (such as between 700-740 nm) and oxygen (around 761 nm, the O2 A-band, and around 687 nm, the O2 B-band). For both spectra, the ozone bands are comparable in depth, indicating that most ozone is situated above the clouds. In contrast, the water vapour and oxygen bands are much deeper for the spectrum of the low cloud than for the high cloud, indicating that most water vapour and oxygen is below the altitude of the highest cloud.

2

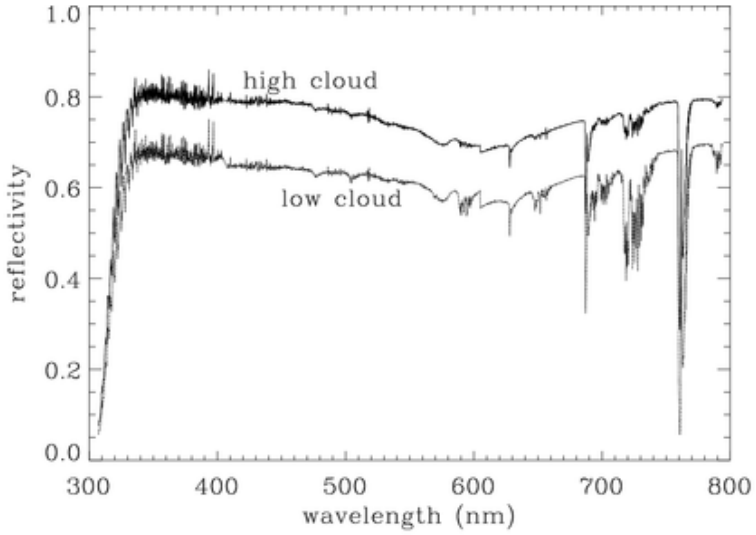

GOME spectral reflectivity measurements made on 23 July 1995, one over high clouds, one over low clouds. The derived cloud fractions and cloud top pressures from FRESCO (ATSR-2) are 0.97 (0.90) and 390 hPa (260 hPa) for the high cloud, and 0.83 (0.77) and 840 hPa (740 hPa) for the low cloud.

Retrieval Method for GOME

The reflectivity in the continuum depends mainly on cloud fraction and cloud optical thickness (or cloud albedo), whereas inside the oxygen A-band it depends on the cloud top pressure as well. In our FRESCO retrieval method, we make use of these dependencies to derive an (effective) cloud fraction and cloud top pressure. We use a simple transmission and reflection model, in which the surface and cloud are assumed to reflect as a Lambertian surface. It is impossible to separate cloud fraction and cloud optical thickness from the GOME measurements in the continuum, because clouds with different optical thicknesses and different cloud fractions may give rise to the same spectral reflectivity. Therefore, we assume a cloud albedo of 0.8 (very thick cloud), and then derive an (effective) cloud fraction from measurements in the continuum. This effective cloud fraction is also the optimum choice for cloud correction of GOME ozone measurements [*Koelemeijer and Stammes*, 1999]. The cloud top pressure is derived from the depth of the oxygen A-band, which depends on the amount of oxygen above the cloud. The difference in the depth of the oxygen A-band for low and high clouds is particularly apparent in Figure 3, in which the reflectivity in the oxygen A-band is shown for the same scenes as Figure 2, normalised by their value outside the band. Since the oxygen total column amount and the oxygen pro le is well known, the cloud top pressure can be derived from the depth of the oxygen A-band.

Retrieval Method for ATSR-2

To derive cloud fraction, a cloud detection algorithm was developed to separate cloud-free and cloudy pixels in ATSR-2 images. The algorithm consists of four threshold tests and is similar to the cloud detection scheme for AVHRR images described by *Saunders and Kriebel* [1988]. For the ATSR-2 pixels inside the GOME pixel, an average (effective) cloud fraction is derived from the 0.66mm channel, assuming a cloud albedo of 0.73 (lower than 0.8, to take account of ozone absorption above the cloud at 0.66mm). To derive cloud top pressure, the 11mm brightness temperatures were converted to pressures using pressure-temperature profiles from the 12 UT analysis of the ECMWF model. Only cloudy ATSR-2 pixels were selected with a brightness temperature difference between the 11mm and 12mm channels of 1K, to ensure that the cloud emissivity is close to unity, and that the measured brightness temperature is representative for the cloud top temperature. Only an average ATSR-2 cloud top pressure is derived for a GOME pixel if the fraction of ATSR-2 pixels with an emissivity close to unity is larger than 15%.

Comparison of Cloud Parameters

The results of the FRESCO and ATSR-2 cloud retrieval methods for the 3500 km long area are shown in Figure 4. For the cloud fractions, shown in Figure 4a, a good correlation is found. For small cloud fractions over land, however, the FRESCO cloud fractions are systematically higher than the ATSR-2 cloud fractions, which is probably due to

3

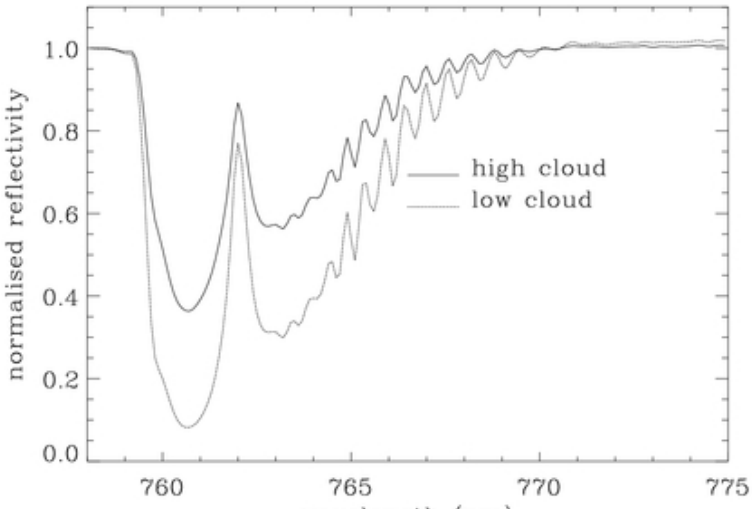

Same spectra as in Figure 2, now zoomed in on the oxygen A-band. The spectra are normalised to unity at 758 nm.

underestimation of the surface albedo by FRESCO. For the cloud top pressures, shown in Figure 4b, a reasonable correlation is found. The random difference between the FRESCO and ATSR-2 derived cloud top pressures decreases as the fraction of ATSR-2 pixels within a GOME pixel which can be used increases. Furthermore, we observed that for clouds with high reflectivity at 0.66mm (optically thick clouds), the difference in derived cloud top pressures is often rather large, whereas for optically thinner clouds, the difference is generally smaller. This may indicate that absorption by oxygen inside clouds, which is not taken into account in our retrieval method, is more important for optically thick clouds than for optically thin clouds.

Conclusion

We have shown that the principle to use the oxygen A-band to derive simultaneously cloud fraction and cloud top pressure from one GOME spectrum works well. One of the applications of the FRESCO cloud fractions and cloud top pressures is cloud correction in the near-realtime ozone column retrieval at KNMI, in the framework of the GOFAP project [*Piters et al.*, 1999].

The FRESCO cloud fractions and cloud top pressures are available near-realtime on the Internet: <www.knmi.nl/neonet/atmo_chem/gome/fd/fresco/fresco.html>.

Acknowledgements

We thank our KNMI colleagues Ankie Piters, Pieter Valks, and Bart van den Hurk for their contributions to this work. We are grateful to ESA for providing the GOME and ATSR-2 data through DLR and ESRIN.

References

Cess, R. D., et al., Intercomparison and interpretation of of climate feedback processes in 19 atmospheric general circulation models, J. Geophys. Res., 95, 16,601-16,615, 1990.

Knap, W. H., Hess, M., Stammes, P., Koelemeijer, R.B.A. & Watts P.D., Cirrus optical thickness and crystal size retrieval from ATSR-2 data using phase functions of imperfect hexagonal ice crystals, J. Geophys. Res., 104, 31,721- 31,730, 1999.

Koelemeijer, R.B.A. & Stammes, P., Effects of clouds on ozone column retrieval from GOME UV measurements, J. Geophys. Res., 104, 8281-8294, 1999.

Piters, A.J.M., Valks, P.J.M., Koelemeijer, R.B.A. & Stam, D.M., GOME ozone fast delivery and value-added products algorithm specification document, Tech. Rep. GOFAP-KNMI-ASD-01, 23 pp., KNMI, De Bilt, The Netherlands, 1999.

Saunders, R.W. & Kriebel, K.T., An improved method for detecting clear sky and cloudy radiances from AVHRR data, Int. J. Rem. Sens., 9, 123-150, 1988.

4

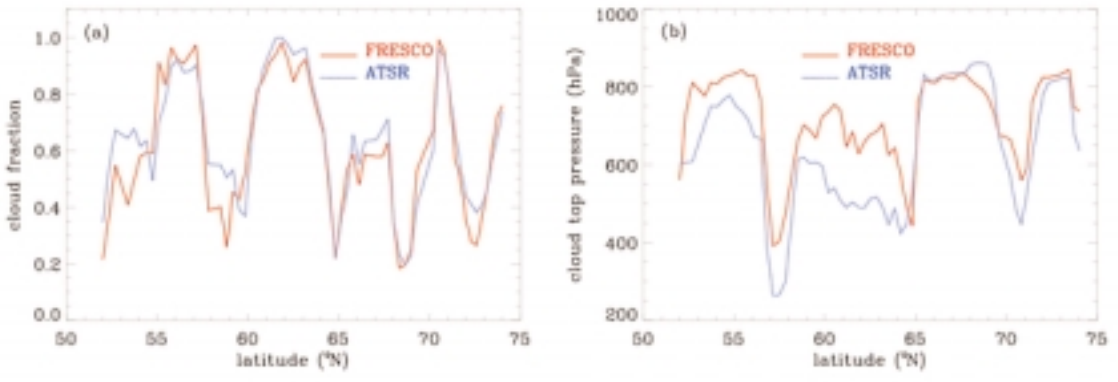

Comparison of cloud fractions (a) and cloud top pressures (b) derived from GOME (using the FRESCO algorithm) and from ATSR-2. The data were acquired on 23 July 1995 between 11:46 and 11:54 UT.

Mapping Forest Damage Caused by the 1999 Lothar Storm in Jura (France), Using SAR Interferometry

E. Dwyer(1), P. Pasquali(1), F. Holecz(1), O. Arino(2)

(1) SARMAP S.A.
Cascine di Barico, 6989 Purasca, Switzerland, www.sarmap.ch
(2) ESA/ESRIN Directorate of Application Programmes
V.Galileo Galilei 00044 Frascati, Italy
E-mail: oarino@esrin.esa.it

The storms which crossed France and central Europe in December 1999 caused loss of life and destruction of infrastructure amounting to millions of Euros. Large areas of forested land were also damaged and destroyed. The results presented here show that coherence information extracted from ERS interferometric image pairs is very effective in differentiating between damaged and undamaged forest. These results were obtained very soon after the storms due to the availability of operational software prepared as part of a Data User Programme contract with ESA.

In terms of coherence imagery, different ground cover types manifest different degrees of coherence. Bare or sparsely vegetated soil has a high degree of coherence as there is little or no change in the scatterer properties between the two acquisitions. Forested areas, on the other hand, show a low degree of coherence, as the elementary scatterers (i.e. leaves) in each pixel move between the two acquisitions, mainly due to wind and, hence, lead to de-correlation in the imagery. This fact can be exploited to discriminate between forest and non-forest vegetation. Moreover, in this case, given two coherence images, one prior to the storm (4/5 April 1999) and one after the storm (9/10 January 2000), a change within forested areas from low coherence to high coherence should be indicative of forest damage. Using the coherence combined with the backscatter data, a supervised classification was carried out to identify forest areas damaged, as well as the other cover types in the scene. The classified image overlayed on a DEM, generated using InSAR techniques, is shown in Figure 1.

1

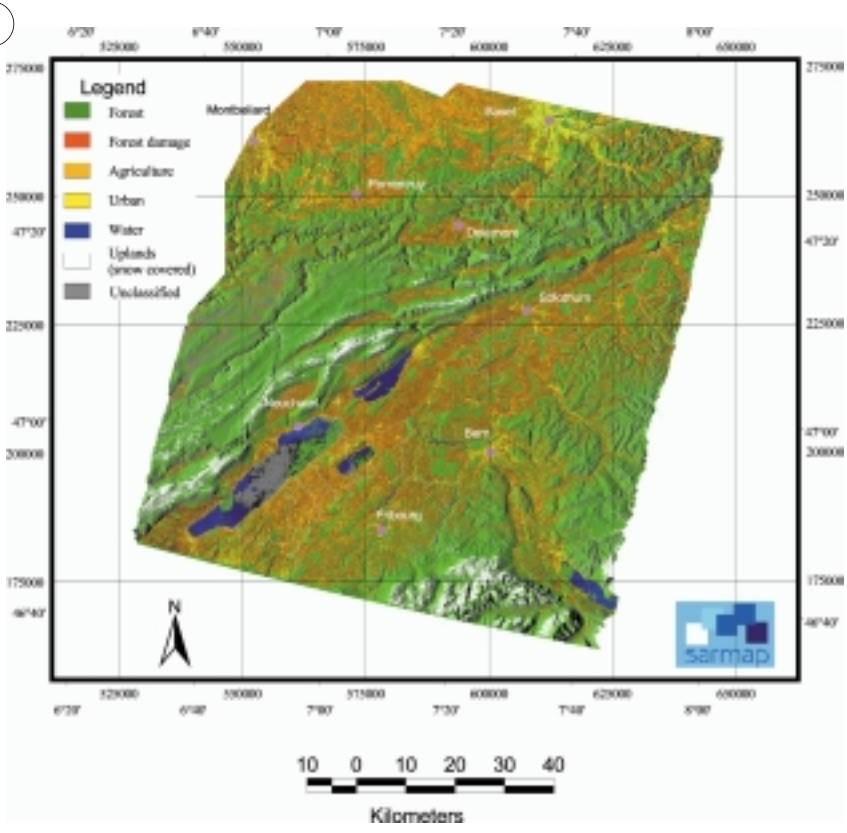

Classified image overlayed on a DEM, generated using InSAR techniques.

Although the extent of forest damage over Switzerland was considerable, the size of the individual areas effected is estimated by the federal forest department to be of the order 2-3 ha. Damaged areas of this size are difficult to detect, as the ERS-SAR spatial resolution of 25 m is degraded to 75 m during the coherence computation. The classification has been more successful where the extent of the damage is greater, as in the Jura region of France, east of Montbeliard. Comparison with the 1/50000 terrain map provided by the Swiss Federal Office of Topography shows excellent agreement of the forest/non-forest mapping by SAR. Field visits to the Jura region confirmed the results over a number of damaged areas, but not those smaller than 2-3 ha. Figure 2 shows the position of the

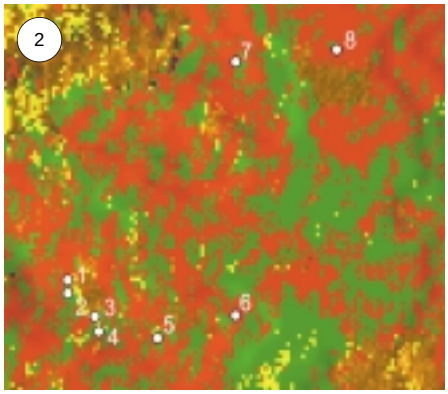

Ground Control Points on the topographic map of the Bois du Fays.

Classification excerpt - Bois du Fays.

Damaged forest in the Jura region.

Ground Control Points on the topgraphic map of the Bois du Fays, whose location is indicated in the rectangle in Figure 1. Figure 3 shows an excerpt of the classification of the same area, with GCP positions indicated. Finally a photo of the damaged forest taken on 7 February 2000 is given in Figure 4 for GCP 4. This indicates the type and extent of the damage.

The excellence of these early results, as well as those presented by other European teams, indicates that recent scientific advances made with radar interferometry have now matured and are ready for operational applications.

Ackowledgments
Swiss Meteorological Service for the meteorological data. The topographic map is copyright of the Swiss Federal Office of Topography.

ESRIN Earth Observation ISO 9001 Certification Activities

Following the positive outcome of the ISO 9001 Certification at ESOC in 1999, it was decided to proceed with the progressive certification of other programmatic areas of activity of the Agency and it was agreed that the next step would be to certify the activities of the Earth Observation Applications Department in the framework of the Directorate of Application Programmes at ESRIN.

The objective of certifying the Earth Observation activities at ESRIN is to improve management efficiency within the Applications Department, to improve its transparency and ability to operate together with commercial partners, and to demonstrate leadership in the field of Earth Observation products and services. Furthermore, the development of a Quality Management System and its implementation will assure that products and services offered by ESRIN meet customer needs and expectations, and improve confidence by these external customers in ESRIN quality practices and guarantee the efficiency of its internal operations.

The exercise started in December 1999 and will cover a time frame of two years. The work will consist of the definition, documentation and implementation of a Quality Management System (QMS) according to the internationally recognised ISO 9001 standard, with special emphasis on process improvement and customer focus. This will include a thorough review of products and services offered by ESRIN as well as working procedures. A Working Group and a Steering Group, including Staff from the Directorate of Applications and other relevant Directorates, have been set up to manage the activity and a Quality Manager is being appointed at ESRIN. A Master Plan, recently agreed by the Steering Committee, will constitute the reference for the activities.

The Working Group will monitor the evolution of the process in compliance to ISO 9001 and an external contractor will also be at ESRIN site to follow the work.

A continuous effort of involvement and information for staff will be engaged with dedicated briefing events, definition of a special website on the intranet where staff can also provide inputs and ask questions, with dedicated strong activities for the staff of the Directorate of Application Programmes according to a communication plan.

Full training will also be granted to all staff of the Department concerned. Main benefits for the staff are expected to be improved decision-making processes, an organisational streamlining and increased motivation.

For more information, consult the website: <www.esrin.esa.it>.

Mapping Forest Damage Using SAR Coherence Product in the Northeastern Part of France

A. Herrmann, K. Fellah, P. de Fraipont & H. Yésou

Service Régional de Traitement d'Image et de Télédétection (SERTIT)
bv Sébastien Brant, F-67 400 Illkirch
Phone: +33 (0) 3 88 65 52 00, Fax: +33 (0) 3 88 65 51 99
E-mail: sertit@sertit.u-strasbg.fr www: http://sertit.u-strasbg.fr

The devastating storms which struck France in December 1999, destroyed the equivalent of several years of normal exploitation (Fig.1). It is of ultimate importance to map the damages for short-term actions as well as for long term reforestation. While it is accepted that coherence images derived from SAR may discriminate accurately forest and non forest area, this novel work based on a multitemporal approach of coherence images demonstrates that coherence can be related to various levels of damage to the forest.

This approach, based on the exploitation of the coherence product developed by Spot Image with the support of ESA, had been carried over the forest of Haguenau, 30 km north of Strasbourg, France's second largest plain forest. The results obtained from the processing of two coherence products derived from two ERS-1/ERS-2 tandem pairs acquired before the storm,on 31 October and 1 November 1999 and after the storm, on 9 and 10 of January 2000, producing maps at 1:25000 scale. These preliminary results were validated by regional forestry services, and will be followed by a more complete and long-term project carried out in collaboration with these services.

Dramatic damage of the December 99 storms within the Haguenau forest.

Coherence can be related with vegetation density: wooden areas generally show low coherence, appearing in green in a stan-dard coherence product, while bare soils and cultivated areas are usually associa-ted with high coherence – orange-red in a coherence standard product (Fig.2). Thus, the coherence product from archive data allows one to separate forest/non-forest areas to be compared with the topographic map, the land use map and the SPOT XS imagery (Figs. 3-5). The coherence product realised after the storm shows a strong increase of the coherence level within forested areas (Fig. 6). A 'damage' image was produced based on the ratioing of the two coherences, and averaged SAR intensity (Fig. 7).

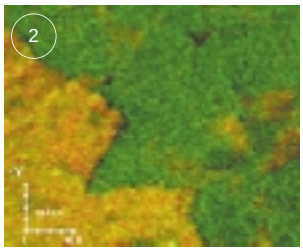

Coherence product before the storm.

Topographic map.

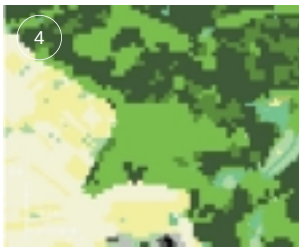

Land cover map.

In the 'damage' image composite, pink tones provide an estimate of the level of the damage. In this case, a level of damage of 50% had been reported by the forest service which corresponds statistically to the increase of coherence over the area.

Acknowledgements
This work was carried out together with Spot Image and with the support of the European Space Agency. ESA organised a special tandem acquisition campaign and provided the ERS data. Spot Image provided the coherence products and triggered the acquisition campaign. SPOT data are property of CNES. Addtionally, authors would like to acknowledge the forestry community for their help during the validation phase.

SPOT XS image.

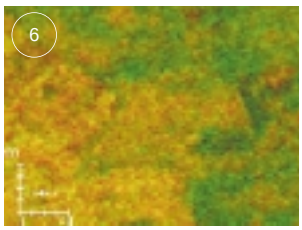

Coherence product after the storm.

Image of damage (affected areas in pink).

ENVISAT Satellite Integration Progress

Since the beginning of last year, the ENVISAT Flight Model Satellite Integration has moved forward steadily. The Flight Model Payload Module (the upper part of ENVISAT where all instruments are accommodated) was integrated in MMS/Bristol in the early part of last year and then transferred to ESTEC in June 1999 (Fig 1).

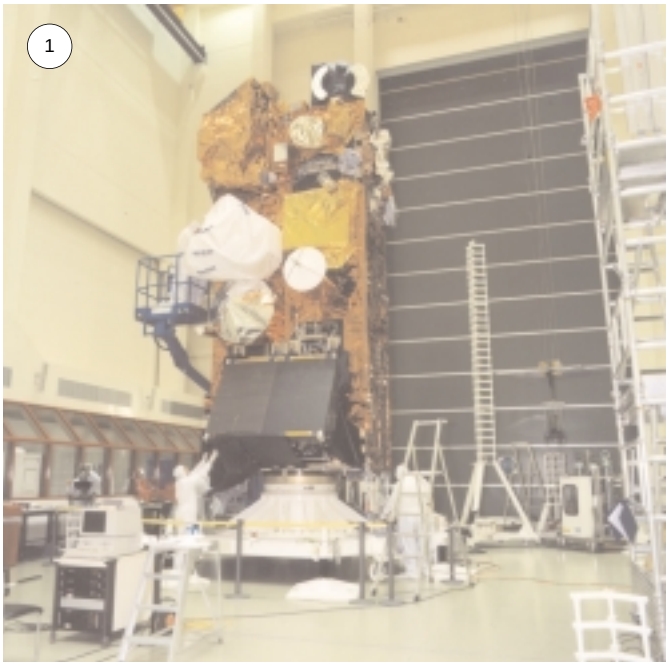

The FM Payload Module of ENVISAT

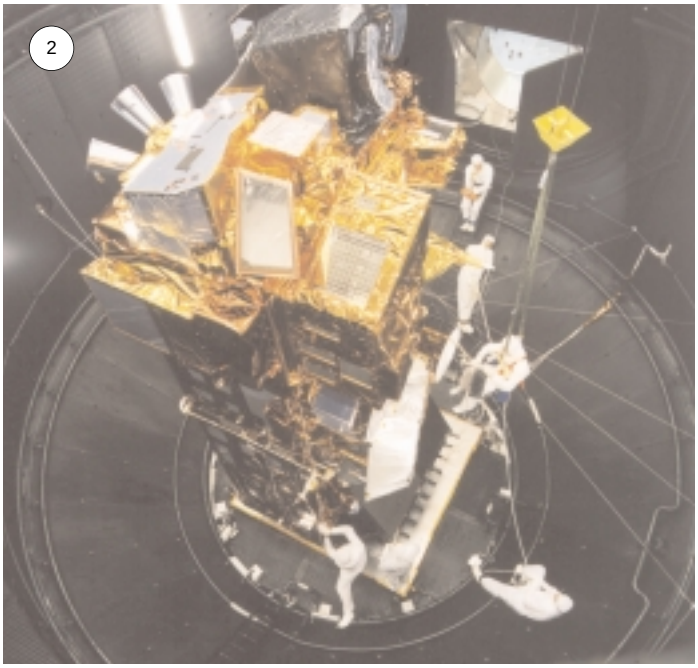

ENVISAT FM Payload Module installed in the ESTEC LSS

In June 1999, the Payload Module (PLM) configuration was not completely flight representative, but was suitable for the forthcoming Thermal Balance and Thermal Vacuum Tests. In particu-lar, the flight models of almost all instru-ments were already successfully integrated (RA-2, SCIAMACHY and ASAR Electronics, GOMOS, MIPAS, AATSR, DORIS and Microwave Radiometer).

The Thermal test took place in July 1999 in the Large Space Simulator in ESTEC (Fig 2). During the test, a small number of problems were identified and subsequently corrected. Also during this period, the Flight Model Instruments which were not available prior to the thermal tests were delivered: MERIS and the SCIAMACHY Optics.

Currently, final deliveries are arriving for the Flight Model Payload Module which will undergo extensive functional, mechanical and electrical tests during the year 2000.

The past activities and the planned testing are designed to verify, in depth, the satellite functional and operational performance, and to satisfy the scientific data quality requirements.

The Flight Model Service Module (the lower part of ENVISAT which provides the satellite support functions), delivered in 1997, has been the object of an important ARIANE 5 shock compatibility test.

The arrival of the Satellite in ESTEC together with an impressive amount of electrical and mechanical ground support equipment was accompanied by the transfer of a large part of the industrial team which will remain on site. The satellite will stay in the integration facilities until launch, thus making ESTEC the main centre of ENVISAT satellite work until its shipment to Kourou, for launch on ARIANE 5.

The schedule of the remaining Assembly, Integration and Test activities has been consolidated recently by industry and, as a result, the ENVISAT target launch date has been set for June 2001.

Conferences 2000

16-20 May – St. Petersburg, Russia
ICS-5: International Conference on Substorms-5
Contact: O. Troshichev
Tel.: +7-812-3521149
Fax: +7-812-3522688
E-mail: olegtro@aari.nw.ru
<http://geo.phys.spbu.ru/ICS5/ICS5.html>

6-10 November – Mar del Plata, Argentina
SPARC 2000
2nd General Assembly of the SPARC project will review current research on the role of the stratosphere in the climate system and in global change. The four sessions will be on the following themes:
– stratospheric processes and their role in climate
– stratospheric indicators of climate change
– modelling and diagnosis of stratospheric effects on climate
– UV observations and modelling.

Abstract deadline: 30 April 2000
E-mail: sparc2000@at1.fcen.uba.ar
<http://www.sparc2000.at.fcen.uba.ar/>

ERS – ENVISAT SYMPOSIUM

'Looking Down to Earth in the New Millenium'

Organised by: ESA and the Chalmers University of Technology

16-20 October 2000 – Gothenburg, Sweden

http://www.esa.int/sympo2000

Contacts:

– for Website aspects, registration, information:
Barbara Scarda, ESRIN
tel. +39-06-94180941
fax +39-06-94180942
E-mail: bscarda@esrin.esa.it

– for Symposium contents:
Gianna Calabresi, ESRIN
tel. +39-06-94180625
fax +39-06-94180552
E-mail: gianna.calabresi@esrin.esa.it

– for Local Support:
Britt-Marie Boisen
Chalmers University of Technology, Gothenburg, Sweden
tel. +46-31-7721840
fax +46-31-164513
E-mail: boisen@rss.chalmers.se

First deadline
(for abstract submission)
is 25 April 2000

Publications

SP-1229: *ENVISAT – MIPAS An Instrument for Atmospheric Chemistry and Climate Research*
(March 2000, 124 pp., 30 Euros)

SP-450: *CEOS SAR Workshop*
Proceedings of the CEOS Working Group on Calibration and Validation: SAR Subgroup, Toulouse, France, 26-29 October 1999.
(April 2000, 40 Euros)

Earth Observation Quarterly
ISSN 0256 - 596X

The EOQ is published quarterly by the ESA Publications Divsion. It is distributed free of charge to all readers who wish to be informed on the evolution of various elements of ESA's Earth Observation Programme.

Advisory Committee:
E. Attema, G. Calabresi, R. Francis, J. Louet, C.J. Readings

Contributors to this Issue (No. 65):
RAL: C.T. Mutlow, D.L, Smith, M.J. Murray & Nigel Houghton
ESA/ESRIN: A. Buongiorno, P. Goryl, E. Doyle, K. Cardon, G.Kohlhammer, I. Piccolini, O. Arino & S. Cheli
DLR/DFD: T. Holzer-Popp, G. Gesell & M. Schroedter
KNMI: R.B.A. Koelemeijer & P. Stammes
SARMAP S.A.: E. Dwyer, P. Pasquali & F. Holecz
SERTIT: A. Herrmann, K. Fellah, P. de Fraipont & H. Yésou

Editor: Dorothea Danesy
Layout & Prepress: Dick Hoette & Dorothea Danesy

For further information, request for free subscription, change of address or purchase of documents, please write to:
'Earth Observation Quarterly'
ESA Publications Division
ESTEC, Keplerlaan 1
2200 AG Noordwijk, The Netherlands
Fax: +31-71-565-5433

ESA Publications Server:
<http://esapub.esa.int/>